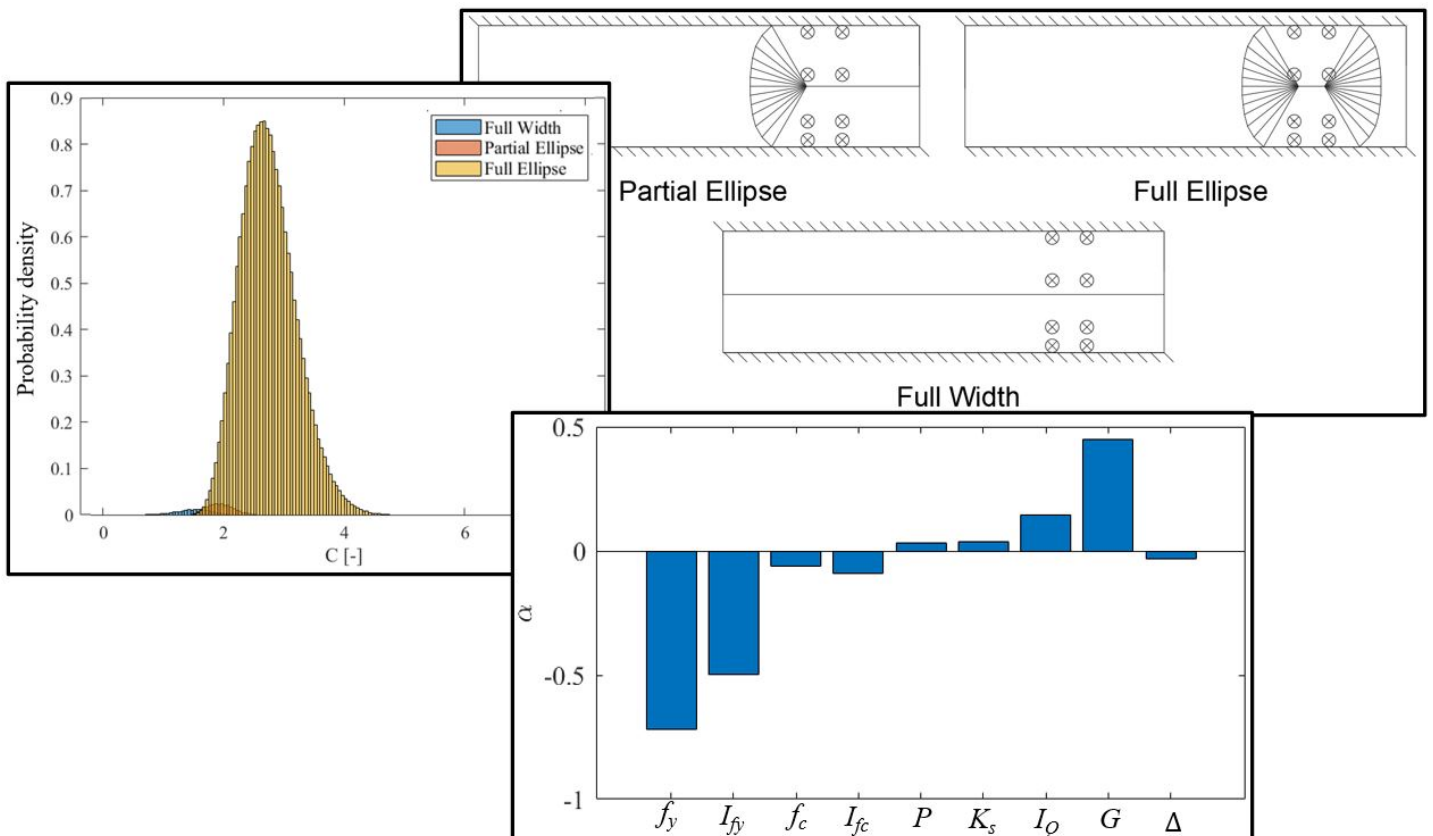


Reliability based classification of existing bridges through upper bound plasticity theorem

Master's thesis

10/6/2020



Student
Kenneth Dahl Schiøttz
Damsgaard

Supervisors
John Dalsgaard Sørensen, AAU
Jannie Sønderkær Nielsen, AAU
Svend Engelund, COWI



AALBORG UNIVERSITET
STUDENTERRAPPORT

MSc. Structural & Civil Engineering

4th Semester

Thomas Manns Vej 23

9220 Aalborg Ø

<http://www.civil.aau.dk/>

Title:

Reliability based classification of existing bridges through upper bound plasticity theorem

Project:

Master's thesis

Project period:

01/09/2019 - 10/06/2019

Author

Kenneth Dahl Schjøttz Damsgaard

Supervisors:

John Dalsgaard Sørensen, AAU

Jannie Sønderkær Nielsen, AAU

Svend Engelund, COWI

Page number: 74

Appendix: 15

Finished 10-06-2020

Abstract:

The purpose of this project is to investigate the applicability of upper bound plasticity theory in classification of existing bridges. Firstly the design basis and load models for existing bridges are presented. After this the bearing capacity model based on upper bound plasticity with the presented load model is developed. The model uncertainty and bias of this bearing capacity model are then quantified. Once the bearing capacity model is described, and the corresponding bias and model uncertainty are quantified, the application of this bearing capacity model for classification of existing bridges can be investigated. Firstly the application of this model will be investigated for deterministic classification based on the partial safety factor method, and the results will be compared to a more traditional model. After this different stochastic models are presented, which are then used to investigate the applications of the bearing capacity model for reliability-based classification. Hereafter the bearing capacity model is used to determine a proof loading factor taking into account the resistance, such that survival of the bridge during proof loading, ensures sufficient reliability. Lastly a decision framework for up-classification is developed.

Preface

This Master's thesis in Structural and Civil Engineering at Aalborg University is written as a long Master's thesis, and therefore consists of 45 ECTS.

Reading guide

This report consist of an introduction, a main report and appendices.

Figures, tables and equations are assigned numbers, where the first number defines the chapter and the second number defines the number of figure, table or equation in the current chapter. Equations are referred to with parenthesis, e.g. (8.2), which is the second equation in chapter 8. The chapters in the Appendix are assigned letters, e.g. Appendix A, and figures, equations and tables in the given appendix chapter are assigned a letter correspondingly, e.g. (B.1), which is the first equation in Appendix B.

Through the report references to sources are made using the Harvard method. A reference in a sentence is written as the authors name followed by the year of publication.

Kenneth Dahl Schiøttz Damsgaard

Resume

Dette kandidatspeciale er udarbejdet i perioden d. 1 september 2019 - d. 10. juni 2020. Det er udarbejdet som det afsluttende projekt på kandidatuddannelsen Structural and Civil Engineering på Aalborg Universitet.

Lastbilerne på de danske veje bliver stadig tungere, og hvis kommunerne og vejdirektoratet ikke gør noget for at sikre en opklassificering langs vejene, kan det resultere i at nogle køretøjer, der ellers kunne have passeret, må tage mere indirekte ruter, eller at virksomheder må placere andetsteds. Hvert år bruger kommunerne og vejdirektoratet millioner af kroner på at forstærke eller udskifte broer, således at disse stadig tungere lastbiler kan passere. Prøvebelastninger på eksisterende broer har dog vist at bæreevnen for mange vejbroer er højere end tidligere antaget, hvilket betyder at der kan være en masse penge at spare på at opklassificere broerne i stedet for at forstærke eller udskifte broen. En opklassificering kan bl.a. ske analytisk ved både deterministisk og pålidelighedsbaseret beregning eller eksperimentelt ved prøvebelastninger.

For pladebroer beregnes momentbæreevnen traditionelt som for en bjælke, hvilket betyder at den tværgående armering ikke indgår i beregningen. For broer med korte spænd kan dette være en meget konservativ beregningsmodel, idet den tværgående armering, grundet pladen med det korte spænds brudform, kan have stor betydning for momentbæreevnen. Tværarmeringens styrke kan dog medtages vha. plasticitetsteori for plader.

Formålet med dette projekt er at undersøge, hvordan en plastisk brudlinjeteori kan benyttes til klassificering af eksisterende broer. Den plastiske brudlinjeteori vil inddrages både til deterministisk og pålidelighedsbaseret bæreevnevurdering, samt til at bestemme den nødvendige størrelse af en prøvebelastning for en eventuel opklassificering.

Første del af rapporten beskriver beregningsgrundlaget samt broen, der vil være udgangspunkt for dette projekt. Hernæst udvikles en metode til bæreevneberegning af pladebroer baseret på brudlinje teori, og beregningsmodellens bias og modelusikkerhed bestemmes. Denne beregningsmodel benyttes da i følgende afsnit til deterministisk bæreevnevurdering af broen, der er udgangspunkt for projektet, og resultatet er holdt op imod resultatet af en traditionel bæreevneberegning. Hernæst beskrives de stokastiske modeller, der benyttes til den pålidelighedsbaserede bæreevnevurdering. Anvendelsen af beregningsmodellen undersøges da til pålidelighedsbaseret bæreevnevurdering, hvor den deterministiske beregning opholdes mod den pålidelighedsbaserede, og hvor et parameterstudie udføres til at bestemme vigtigheden af relevante parametre. Teorien fra den pålidelighedsbaserede bæreevnevurdering benyttes hernæst til sidst til at bestemme den nødvendige størrelse af prøvebelastningen, der sikrer at den ønskede pålidelighed er opnået, og beslutningsgrundlaget for prøvebelastningen undersøges.

Contents

I	Introduction	
1	Introduction	3
1.1	Problem statement	4
1.2	Problem limitations	5
II	Main Report	
2	Design basis	9
2.1	Procedure for classification and bearing capacity assessment	9
2.2	Basis for calculation	11
3	Base case - Østerå Bridge	13
4	Load models	17
4.1	Position of traffic load	17
4.2	Quantification of traffic load	19
5	Plastic upper bound slab theory	23
5.1	Yield moment of cross section	23
5.2	Application of upper bound slab theory for bridges	25
5.3	Parameter study	27

6	Quantification of model uncertainty	33
6.1	Model uncertainty from the standard procedure in [DS/EN-1990, 2007]	34
7	Deterministic analysis	37
8	Stochastic modelling	39
8.1	Load model	39
8.2	Material model	42
8.3	Applied stochastic models	45
9	Reliability analysis	47
9.1	Reliability method	47
9.2	Reliability analysis	47
9.3	Parameter study	51
10	Proof loading	59
10.1	Without prior knowledge on resistance	59
10.2	With prior knowledge on the resistance	61
11	Decision framework for proof loading	67
11.1	Parameter study	70
12	Conclusion	71
	Literature	73

III

Appendix

A	Axle configuration for standard vehicles	77
B	Bearing capacity calculation example	79

C	Cases for determination of model uncertainty	83
D	Proof load factor for existing structures	87
E	Calculation of expected cost	89



Introduction

1	Introduction	3
1.1	Problem statement	
1.2	Problem limitations	

1. Introduction

For many existing reinforced concrete slab bridges, the bearing capacity found from theoretical models does not correspond with the actual bearing capacity. This is seen through failure tests performed on existing bridges. Through these tests the actual bearing capacity was found to be much larger than the theoretical bearing capacity, in some cases with a factor 2 or higher. In practice many existing short span bridges could therefore be under classified due to the uncertainty and conservatism of the applied model. [Andersen, 2017]

There is a wish for up-classification of many existing bridges, such that it allows for passage of heavier vehicles. An up-classification of these bridges may allow for some vehicles to take more direct routes cutting down the transport cost of the companies using these heavier vehicles. Moreover an up-classification of an existing bridge in favor of the erection of a new bridge is more sustainable and more socioeconomically sound.

Using the traditionally used bearing capacity model, which does not take into account the transverse reinforcement, the bearing capacity of short span bridges might be calculated conservatively. Since these bridges are short but wide and as they are reinforced both in the longitudinal and transverse directions, their actual bearing capacities might differ from the calculated due to negligence of effect from transverse reinforcement. A more precise model taking into account the transverse reinforcement might be based on upper bound plasticity theory, for which the bearing capacity is based on specific failure mechanisms.

When performing up-classification of an existing bridge, it should be proven that the reliability of the bridge with the new classification meets the demands of existing codes and norms. If this can't be done analytically it can be done experimentally by proof loading, where the bridge is loaded such that the proof load case corresponds to the real load case securing the desired reliability. However proof loading tests can lead to failure of the bridge, if the load to be proven exceeds the actual bearing capacity of the bridge. Therefore the decision on whether to proof load or not should take into account the probability of failure during the proof load.

An existing short span bridge, which might have the possibility of up-classification, is the bridge above Østerå on the Mariendals Mølle motorway in Aalborg, which was erected in 1973. The location of this bridge can be seen from Figure 1.1. The bridge will be designated "Østerå bridge" in this report.

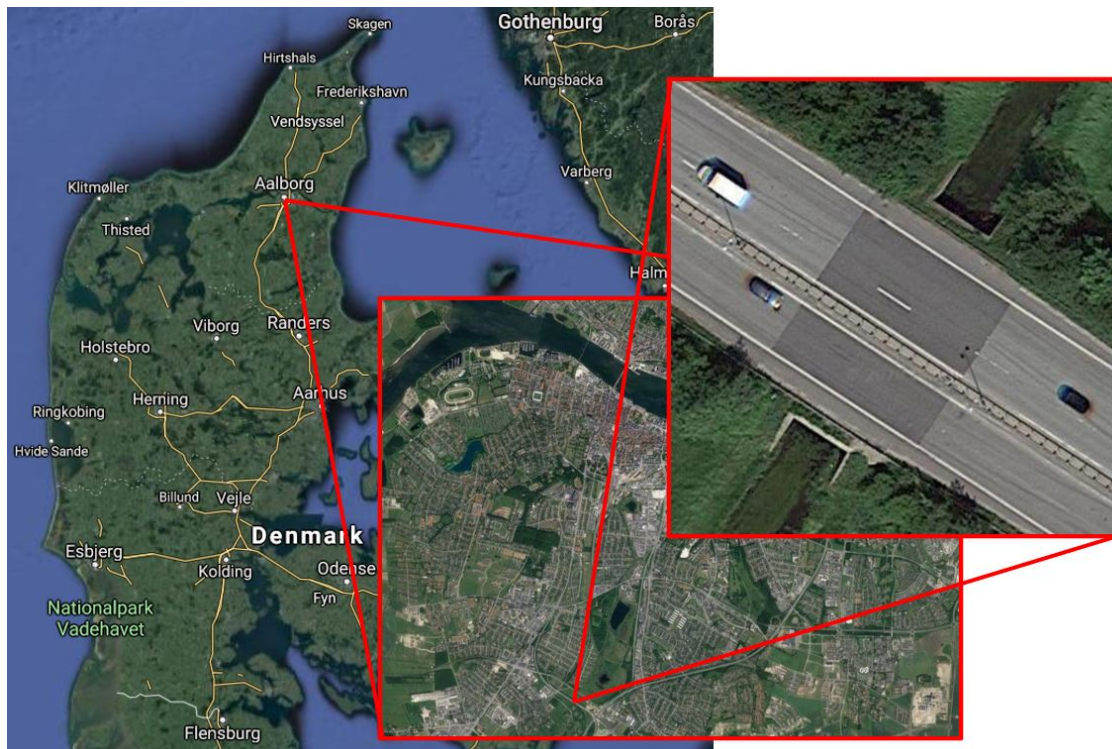


Figure 1.1: Location of Østerå bridge. [Google, 2020, edit]

1.1 Problem statement

Throughout this chapter it has been described how there is a wish for up-classification of some existing bridges. This might be possible through proof load testing, where a proof load factor is determined based on an upper bound bearing capacity model, such that the required reliability level is proven, if the bridge survives the proof load test. This reduces to the problem statement:

How can plastic upper bound bearing capacity models be applied for deterministic and reliability-based bearing capacity assessment, and how can this be used with proof load testing for classification of existing short-span bridges?

The above problem statement will be answered by:

- Establishing the design basis for classification of existing bridges.
- Describing the bridge, which will be the base case for this project.
- Establishing the load models, which are to be used for bridges.
- Developing a model, based on upper bound plasticity theory, for determining the bearing capacity of bridges.
- Quantifying the model uncertainty and bias of the developed bearing capacity model.
- Performing deterministic bearing capacity assessment, using partial safety factor method.
- Describing the stochastic models, which are to be used for reliability-based assessment in the following chapter.

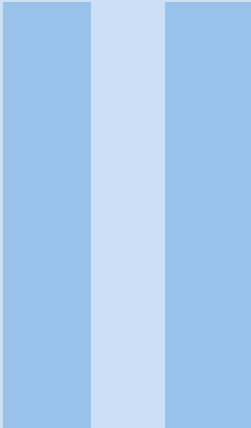
- Describing and performing reliability-based bearing capacity assessment
- Determining how large a proof load should be to secure sufficient reliability if the bridge survives the proof load test, and moreover determining the probability of the bridge not surviving the proof load test.
- Developing a decision framework for proof load testing taking into account the probability of the bridge not surviving the proof load test, found in the previous chapter.

Østerå bridge will be the base case for this report, but more generic investigations will also be performed. This will be done through parameter studies in relevant chapters, where the effect of changing different parameters is investigated.

The bearing capacity model developed in this project will be compared to a more traditional model in relevant chapters.

1.2 Problem limitations

The bearing capacity model investigated is based on yield line theory. Therefore the up-classification is only based on the ultimate moment bearing capacity of the slab. This means that the serviceability limit state or other ultimate bearing capacities, such as shear capacity, are not investigated. This also means that other components, such as walls and piles, will not be proven for the up-classification. In recent years the rules for shear capacity calculations have been sharpened, which means that this is often the critical limit state for the slab when performing calculation-based bearing capacity assessment of older existing bridges. This might mean that this limitation is significant in design. However it might not be the case in practice, and since this project investigates up-classification based on proof load testing, it might still be relevant to investigate the ultimate moment bearing capacity.



Main Report

2	Design basis	9
2.1	Procedure for classification and bearing capacity assessment	
2.2	Basis for calculation	
3	Base case - Østerå Bridge	13
4	Load models	17
4.1	Position of traffic load	
4.2	Quantification of traffic load	
5	Plastic upper bound slab theory	23
5.1	Yield moment of cross section	
5.2	Application of upper bound slab theory for bridges	
5.3	Parameter study	
6	Quantification of model uncertainty	33
6.1	Model uncertainty from the standard procedure in [DS/EN-1990, 2007]	
7	Deterministic analysis	37
8	Stochastic modelling	39
8.1	Load model	
8.2	Material model	
8.3	Applied stochastic models	
9	Reliability analysis	47
9.1	Reliability method	
9.2	Reliability analysis	
9.3	Parameter study	
10	Proof loading	59
10.1	Without prior knowledge on resistance	
10.2	With prior knowledge on the resistance	
11	Decision framework for proof loading	67
11.1	Parameter study	
12	Conclusion	71
	Literature	73

2. Design basis

Before the start of any project it is important to note the codes and standards, which should be applied as basis of design. In this project the design basis is based on the manual "Vejledning til Belastnings- og beregningsgrundlag for broer" [Vejdirektoratet, 2017]. This manual is a summary of the bridge applicable points in existing Eurocodes with related national annexes and the report "Reliability-Based Classification of Load Carrying Capacity" along with instructions, which are not found in any of these. In this chapter, the applied key points from this manual will be mentioned.

2.1 Procedure for classification and bearing capacity assessment

The procedure for classification and bearing capacity assessment for existing bridges is described in DS/EN 1991-2 DK NA, Annex A. The eurocodes released at the time of this project are generally for the design of new structures, with one exception being this annex, which is specifically for existing bridges. However in this Annex, there is no mention of classification based on proof loading, which will also be investigated in this project. Instead the basis for the proof loading will be drafts for the eurocodes, which are, at the time of this project, being revised for new eurocodes for bearing capacity assessment of existing structures.

In DS/EN 1991-2 DK NA, Annex A the general procedure, types of bearing capacity assesment, classification of vehicles and passage types are outlined. DS/EN 1991-2 DK NA, Annex A lists three types of bearing capacity assesment:

1. Classification of bridges using standard vehicles
2. Signage of weak bridges using boundary vehicles
3. Direct bearing capacity assesment using actual vehicles

This project is based on point 1, classification of bridges using standard vehicles. Figure 2.1 shows the general principle for bearing capacity assesment with the procedure for bridge classification, which is investigated in this project, highlighted in red.

The terms, such as normal passage, in Figure 2.1 will be described in following chapters.

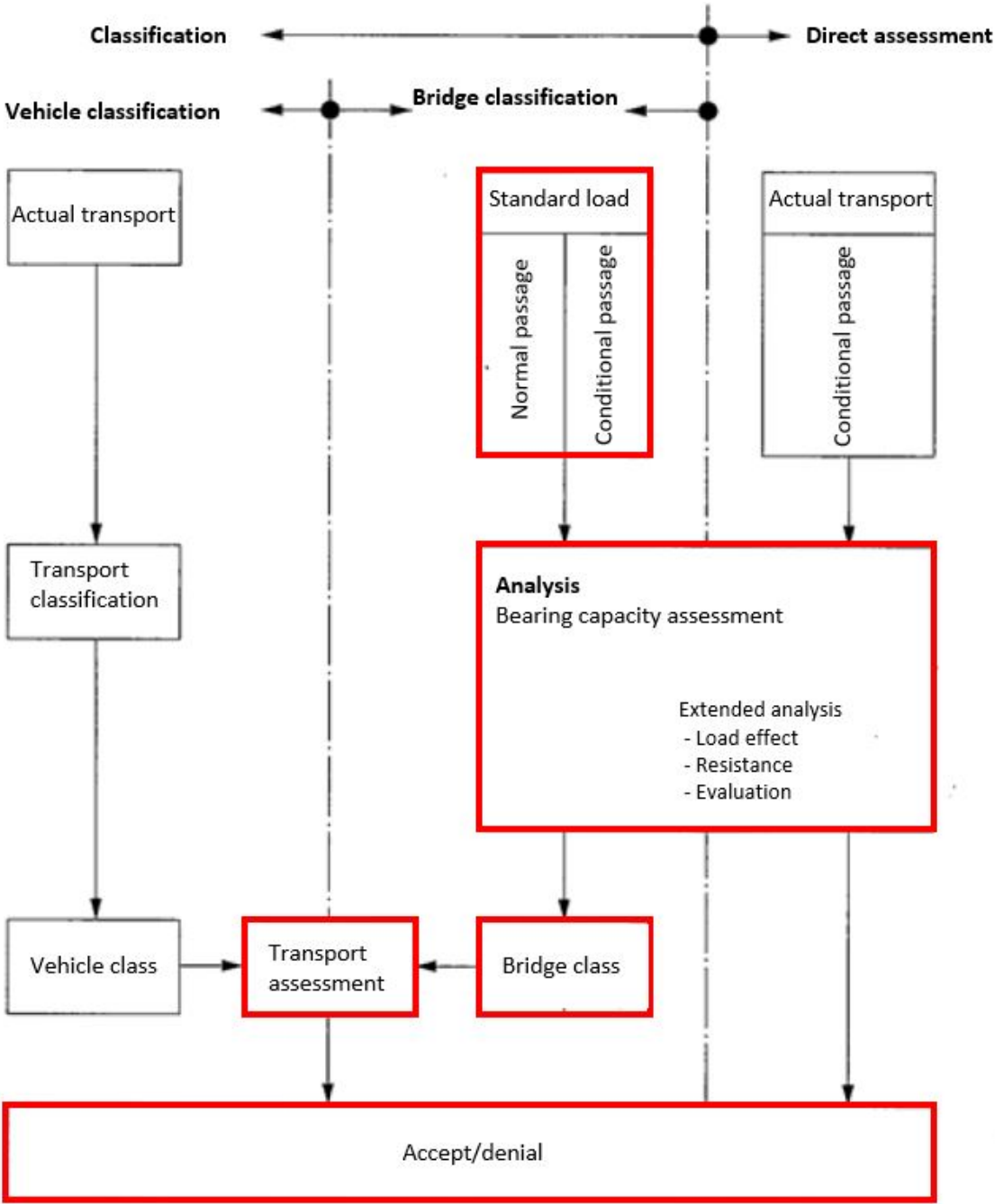


Figure 2.1: Bearing capacity assessment of bridges.[DS/EN 1991-2 DK NA:2017, 2017, edit]

2.2 Basis for calculation

The general safety requirements for road bridges are stated in DS/EN 1990 incl. DK NA along with DS/EN 1990/A1 incl. DK NA. According to [Vejdirektoratet, 2017] all bridges spanning more than 6 m fall under Consequence Class 3, CC3, while bridges with shorter span fall under CC2.

Partial safety factors for loads and load combinations, which are to be applied, are found in DS/EN 1990/A1 Annex A2 DK NA. The load combinations to be investigated in the ultimate limit state are EN1990: STR (6.10a) and (6.10b), which correspond to (2.1) and (2.2), respectively.

$$G_k \gamma_{Ga} \quad (2.1)$$

$$G_k \gamma_{Gb} + Q_k \gamma_Q \quad (2.2)$$

G_k	Characteristic permanent load
γ_G	partial safety factor for permanent load
Q_k	Characteristic traffic load
γ_Q	partial safety factor for traffic load

partial safety factors for material strengths are found in DS/EN 1992-1-1 DK NA. The partial safety factors for both material strengths and loads can be seen in Table 2.1, where γ_{Ms} and γ_{Mc} are the partial safety factors for reinforcement steel and concrete, respectively. The value for γ_Q listed in the table is for classification of existing bridges. For design of new bridges $\gamma_Q = 1.4$

Table 2.1: partial safety factors.

partial safety factor	Value
γ_{Ga}	$1.2 K_{FI}$
γ_{Gb}	$1.0 K_{FI}$
γ_Q	$1.25 K_{FI}$
γ_{Ms}	$1.2 \gamma_3^{(1)}$
γ_{Mc}	$1.45 \gamma_3^{(1)}$

⁽¹⁾ γ_3 is dependent on control class for the material.

K_{FI} depends on the consequence class. For CC2, $K_{FI} = 1.0$ and for CC3, $K_{FI} = 1.1$

For existing bridges up-classification can be performed using other reliability methods than the partial safety factor method. The reliability requirements for existing bridges are given in Table 2.2. In this report only global failure in ULS will be investigated. The values in Table 2.2 are usually used for new buildings in CC2, but for existing bridges, these can be used for CC3.

This project investigates the bearing capacity for concrete bridges. Bearing capacity

Table 2.2: Reliability requirements. Vejdirektoratet [2017]

Limit state	Reliability index β (1 year)	Probability of failure
ULS, global failure with warning	4.8 (Without warning: 5.2)	10^{-6}
ULS, local failure	4.3	10^{-5}
Fatigue	4.8	10^{-6}
Fatigue, where joints can be inspected and repaired	4.3	10^{-5}
Comfort requirements	2.3	10^{-2}
SLS	2.3	10^{-2}

calculations for concrete structures should be performed in accordance with DS/EN 1992-1-1 incl. DK NA og DS/EN 1992-2 incl. DK NA.

3. Base case - Østerå Bridge

As mentioned in the introduction, Østerå Bridge will be the base case for this report. The road way on Østerå bridge is made up of 3 vehicle lanes and a shoulder in the direction of Aalborg, and 2 vehicle lanes and a shoulder in the other direction. Figure 3.1 shows how the roadway on Østerå bridge is structured, which, as will be shown in Chapter 4, is important for the load model.

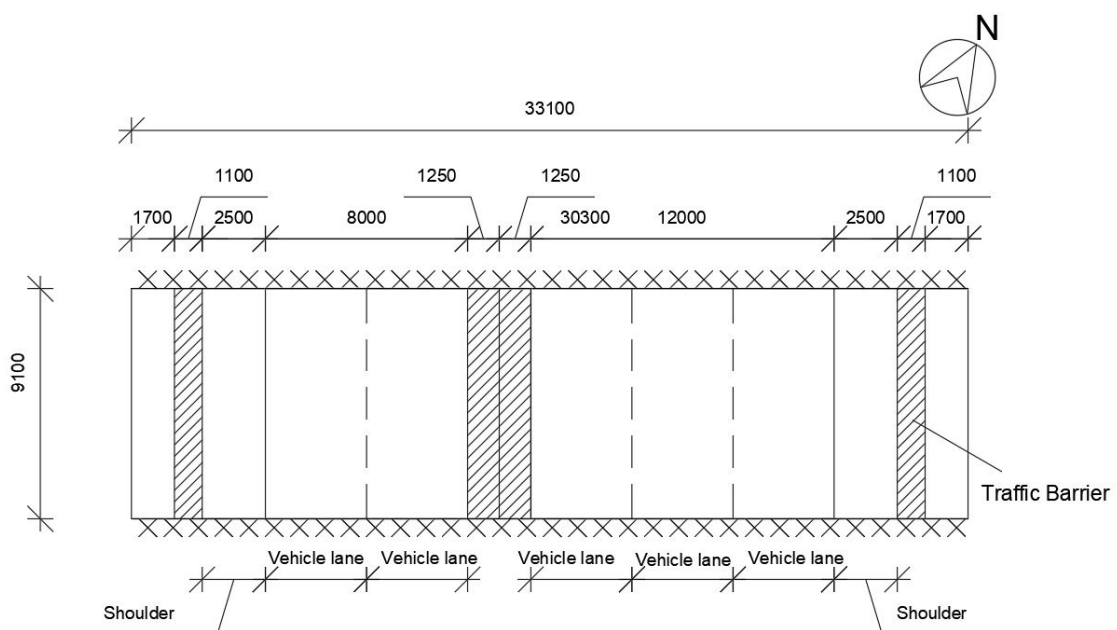


Figure 3.1: Illustration of the roadway on Østerå bridge.

The main part of the slab for Østerå Bridge is flat with uniform thickness, but the thickness increases near the free edges of the bridge and the reinforcement changes as well. This change in thickness is illustrated in Figure 3.2.

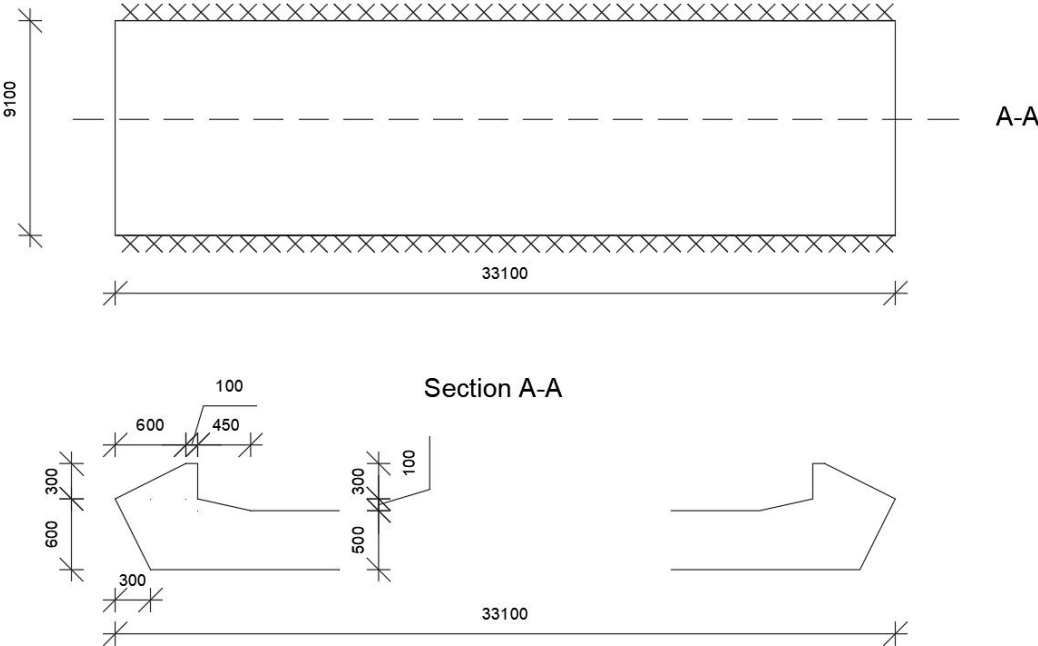


Figure 3.2: Illustration of free edges at Østerå bridge.

The increased bearing capacity from the increased thickness is assumed negligible, and the slab is simplified into a slab with uniform thickness and with the reinforcement pattern as the main part, but for the whole slab. The slab is assumed fixed in both ends since this was assumed for the original calculations. The static system of the slab with reinforcements is illustrated in Figure 3.3.

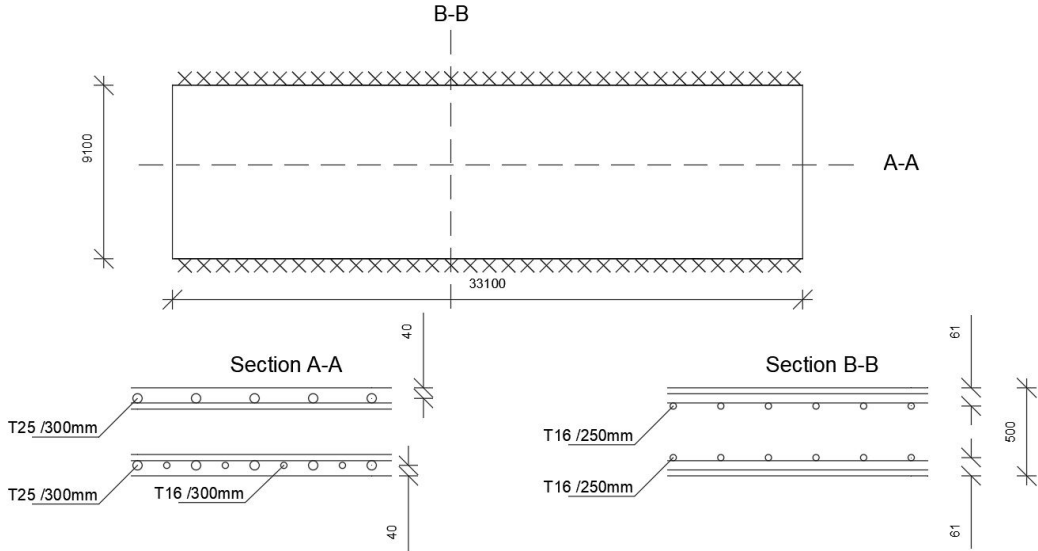


Figure 3.3: Illustration of simplified cross section for Østerå bridge.

Østerå bridge was erected in 1973 meaning that the strength of the materials given in the static calculations documents in the design are based on [DS 411:49]. The strength parameters given for the slab in the design calculations can be seen from Table 3.1

Table 3.1: Strength parameters for Østerå Bridge, given in the original design calculations.

Strength parameter		Value
Reinforcement strength, Tentor steel	r_j	2300 kg/cm ²
Concrete cylinder strength	σ_c	240 kg/cm ²

For materials specified in [DS 411:49] the strength values for up-classification should be based on Table 3.2 and 3.3, for reinforcement and concrete, respectively. The characteristic value for the concrete strength is found as the 5 % fractile.

Table 3.2: Tensile yield stress of non-prestressed reinforcement. [Vejdirektoratet, 2004]

Steel type	Symbol	Diameter [mm]	Mean [MPa]	STD [MPa]	Characteristic [MPa]
Smooth bars	Fe 360	≤ 16	304	25	235
	Fe 360	> 16	293	25	225
	Fe 430	≤ 16	345	25	275
	Fe 430	> 16	334	25	265
	Fe 510	≤ 16	426	25	355
	Fe 510	> 16	416	25	345
Smooth bars	Ks 410	-	482	25	410
	Ks 550	-	623	25	550
Tentor steel	T	-	623	25	550

Table 3.3: Mean value and coefficient of variation for compressive concrete strength corresponding to cylinder strengths specified in [DS 411:49]. [Vejdirektoratet, 2004]

σ_c [kg/cm ²]	μ_{f_c} [MPa]	V_{f_c}
100	8.0	0.18
150	12.0	0.18
200	16.0	0.18
250	21.0	0.18
300	25.2	0.18
350	29.4	0.18
400	33.6	0.18

The values for Tentor steel in Table 3.2 is used for the reinforcements. For the concrete strength the μ_{f_c} is found from interpolation of Table 3.3 to 20 MPa.

In the original static documents for Østerå Bridge the control class for materials as given as sharpened. This means that $\gamma_3 = 0.95$ can be used for γ_M in Table 2.1.

The total permanent load from both the slab itself and from the layers above it like gravel and cement are given as 3.62 t/m² in the static calculations for Østerå bridge. This corresponds to 35.6 kN/m² and is assumed as the mean permanent load, which is also the characteristic value.

4. Load models

The load model used for up-classification of bridges should be based on existing codes and annexes. The load model used in this report is based on [DS/EN 1991-2 DK NA:2017, 2017], which states that snow load and wind load can be disregarded for classification of bridges. Thereby the only loads to be taken into account are traffic load and permanent load. Firstly the positioning of the traffic load is described, and then the traffic load is quantified.

4.1 Position of traffic load

The traffic load model in [DS/EN 1991-2 DK NA:2017, 2017] consists of standard vehicles which are applied as point loads for each wheel and ordinary traffic which is applied as a uniformly distributed load. [DS/EN 1991-2 DK NA:2017, 2017] defines the load model based on two traffic situations:

- Passage situations. The load effect is based on only one vehicle in each lane. This situation is typical for short span bridges.
- Mixed traffic situations. The load effect is based on mixed traffic in the same lane as the standard vehicle as well as in other lanes. This situation is typical for long-span bridges.

As this report investigates the bearing capacity and up-classification of short span bridges, only passage situations are investigated. Furthermore ordinary traffic is assumed negligible in comparison to the much larger standard vehicle. Therefore situations with traffic loads only consisting of standard vehicles are investigated in this report. The load model should consist of a standard vehicle A in the most dangerous lane and a standard vehicle B in the second most dangerous lane. Standard vehicle A should correspond to the vehicle class for which the bridge is to be proven. In the case of standard vehicle A being in class 50 or lower, standard vehicle B is the same. In the case of standard vehicle A being in class 60 or higher, standard vehicle B is a class 50 standard vehicle. The vehicle classes along with the corresponding axle configurations and vehicle widths can be seen in Appendix A.

The position of the traffic load is defined on the basis of loading lanes and vehicle lanes. Loading lanes are 3 m wide lanes within the roadway, which includes both shoulders and vehicle lanes. Figure 4.1 illustrates this.

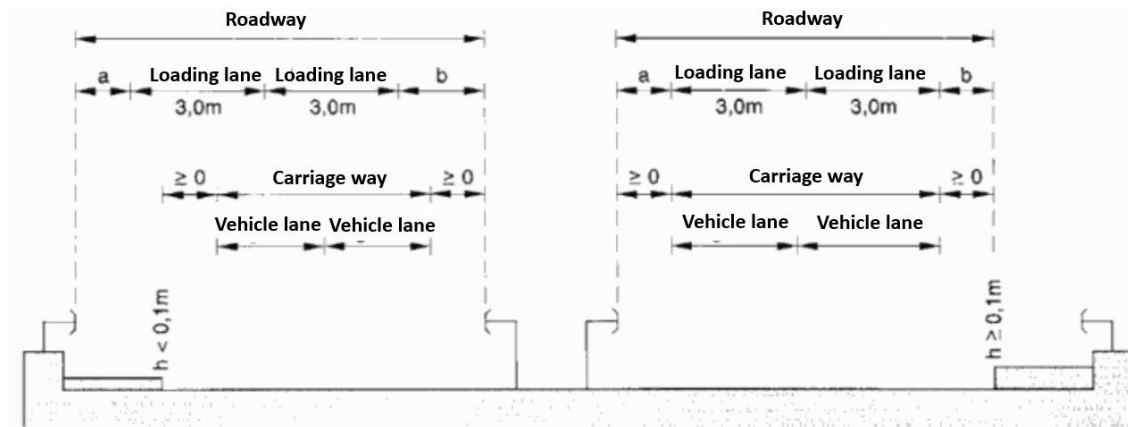


Figure 4.1: Descriptive illustration for lane types. [DS/EN 1991-2 DK NA:2017, 2017, edit]

The traffic load, Q , is determined based on the annual extreme vehicle weight, P . When the standard vehicle crosses the bridge a dynamic factor, K_s , is introduced. The annual extreme traffic load is found as the multiplication of the annual extreme vehicle weight and the dynamic factor. The characteristic value of the annual extreme traffic load is found by (4.1).

$$Q_k = P_k K_{s,k} \quad (4.1)$$

The characteristic dynamic factor is dependent on the influence length, L_{inf} . It is found by (4.2).

$$\begin{aligned} K_{s,k} &= 1.25 & L_{inf} &\leq 5\text{m} \\ K_{s,k} &= 1.25 - (L_{inf} - 5\text{m})/225.5\text{m} & 5 < L_{inf} < 50\text{m} \\ K_{s,k} &= 1.05 & L_{inf} &> 50\text{m} \end{aligned} \quad (4.2)$$

For ultimate moment bearing capacity assessment of a bridge slab, the span of the slab can be used as L_{inf} , which gives $K_{s,k} = 1.23$

The annual extreme vehicle weight and the position of the standard vehicles depend on the passage situation. Four passage situations might be investigated:

- Normal passage. There are no restrictions. Standard vehicle A is placed in the most dangerous loading lane and standard vehicle B in the second most dangerous loading lane. Both are placed in the middle of their respective loading lanes.
- Conditional passage 1. Vehicles are restricted to the existing vehicle lanes. Standard vehicle A is placed in the most dangerous vehicle lane and standard vehicle B in the second most dangerous vehicle lane. Both are placed in the most dangerous position within their respective vehicle lanes
- Conditional passage 2. Like conditional passage type 1 but with a restriction on the speed of standard vehicle A of 10 km/h. The restricted vehicle speed means that dynamic effects can be neglected.

- Conditional passage 3. Like conditional passage 2, but only standard vehicle A is allowed to cross the bridge. Standard vehicle A is placed in the least dangerous vehicle lane.

Østerå bridge is classified differently depending on the passage situation:

- Normal passage: Class 100
- Conditional passage type 1: Class 100
- Conditional passage type 2: Class 125
- Conditional passage type 3: Class 150

In this report the normal passage situation will be investigated but it will be limited to only Standard vehicle A. This might be a significant simplification and for a real case, the loading model should of course follow the guidelines of the existing codes and annexes.

As mentioned earlier Standard vehicle A should be positioned in the center of the loading lane in normal passage. It is assumed that the wheels of the standard vehicles have a width of 600 mm. Therefore 600 mm should be subtracted from the widths given in Appendix A when determining the lateral spacing between the point loads of the two wheels.

In Figure 4.2 Østerå bridge is shown loaded by a standard vehicle in the center of the most dangerous loading lane, which is the most outer loading lane.

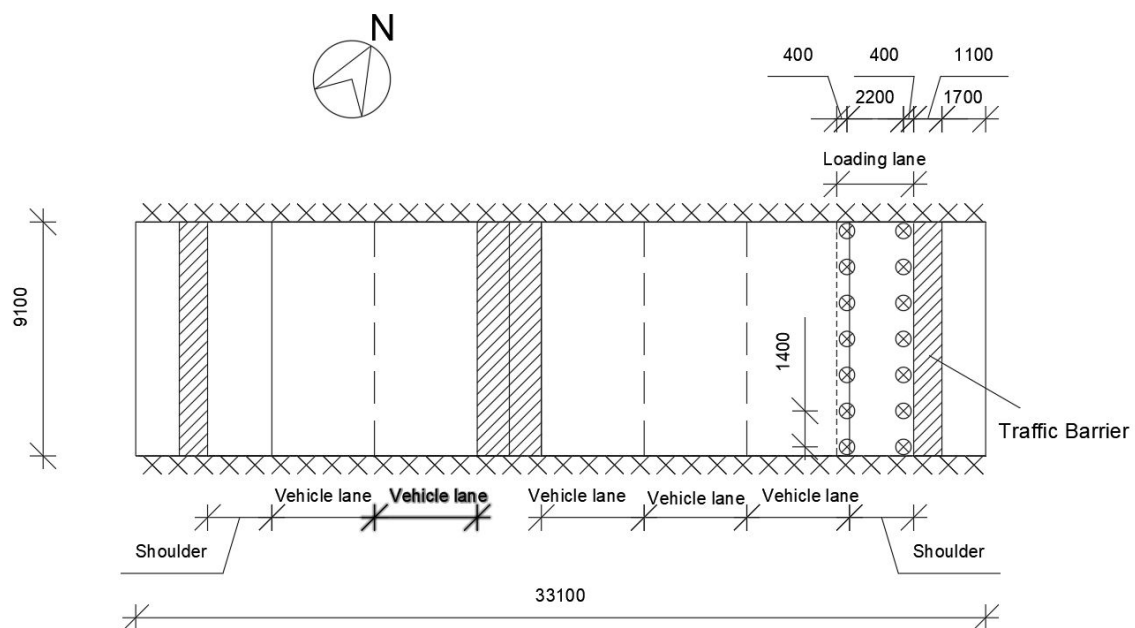


Figure 4.2: Applied forces from standard vehicle A. The axle configuration of standard vehicle A corresponds to the 7 rear axles of class 150 and up. Measurements are in [mm]

4.2 Quantification of traffic load

As the traffic load is simplified to the traffic load effect from the standard vehicle in only one lane, the annual maximum traffic load from standard vehicles will be calculated as for conditional passage type 3 by (4.3). However conditional passage implies a velocity

of $V = 10\text{km/h}$, which makes the dynamic effect negligible [DS/EN 1991-2 DK NA:2017, 2017]. Although the extreme distribution is calculated as for conditional passage, a dynamic effect will still be multiplied to the annual extreme vehicle weight.

$$F_P(x) = \exp(-N_i(1 - F_W(x))) \quad (4.3)$$

Where:

$F_P(x)$	Extreme distribution for vehicle weight
$F_W(x)$	Distribution of vehicle weight for individual vehicles
N_i	Number of vehicles in the reference period (1 year).

The weight of standard vehicles, W , is assumed to be normally distributed with parameters as shown in Table 4.1.

Table 4.1: stochastic parameters for standard vehicles. The number of vehicles corresponds to motor ways

Standard vehicle	Mean [tons]	Standard deviation [tons]	Number of vehicles
Class 50	53.1	5.0	200
Class 60	63.4	5.0	200
Class 70	72.2	5.0	200
Class 80	82.5	5.0	150
Class 90	95.4	5.0	150
Class 100	109.2	5.0	100
Class 125	131.4	5.0	50
Class 150	157.6	5.0	50
Class 175	170.2	5.0	50
Class 200	201.0	5.0	50

The effect of the annual extreme distribution function can be seen from Figure 4.3 and 4.4, which illustrate the probability density function and the cumulative distribution function for the weight of both individual class 50 and 200 standard vehicles, and for the annual extreme. In the figures W and P are divided by μ_W for easier comparison of the two vehicle classes.

As can be seen from Figure 4.3 and 4.4 the coefficient of variation is of course larger for class 50 standard vehicles than for class 200, since the standard variation is equal for the two classes. It is also seen that μ_P is larger compared to μ_W for class 50 than for class 200, which is both due to the higher number of vehicles per year for class 50 than for class 200 and the larger coefficient of variation. The 98 % fractile of P , which is the characteristic value, is therefore also larger compared to the mean value of W , for class 50 than for class 200. For class 50 $P_{0.98} = 1.35 \mu_W$ and for class 200 $P_{0.98} = 1.08 \mu_W$.

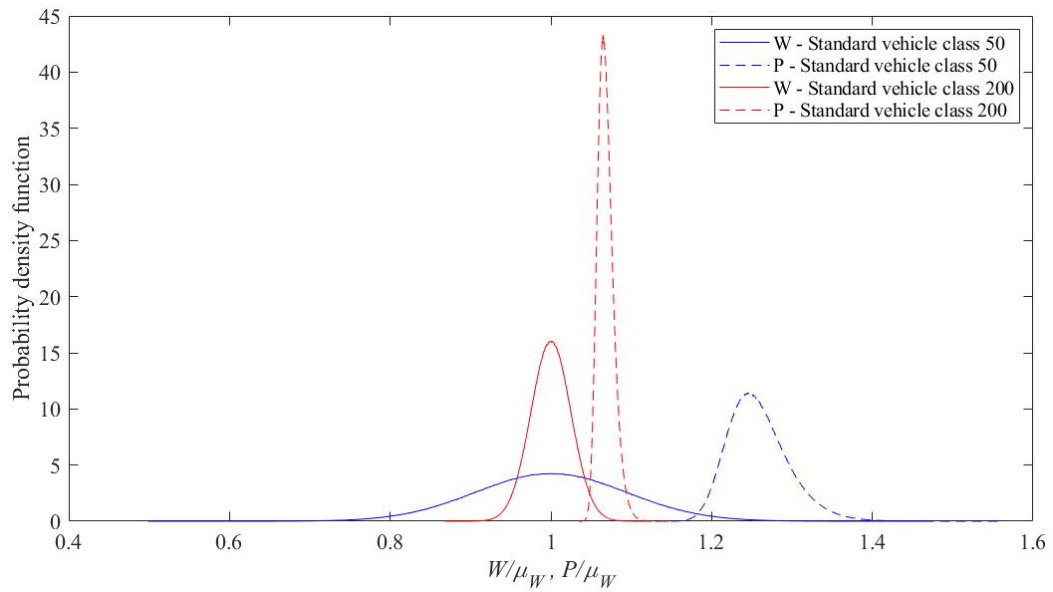


Figure 4.3: Probability density function for total weight of a class 50 and 200 standard vehicle. Both for individual vehicle weight, W , and for the annual extreme vehicle weight, P .

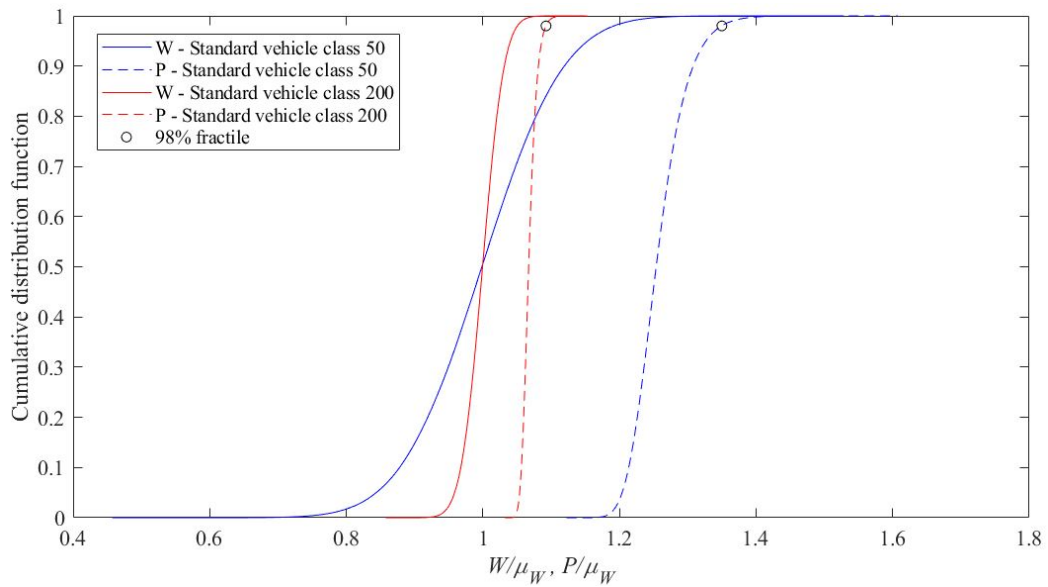


Figure 4.4: Cumulative distribution function for total weight of a class 50 and 200 standard vehicle. Both for individual vehicles, W , and for the annual extreme, P .

5. Plastic upper bound slab theory

The bearing capacity model developed in this chapter is based on plastic upper bound theory with load models as described in Chapter 4. Plastic upper bound theory for slabs is based on the yield moment of the cross section. Therefore it is first shown, how the yield moment is determined. Next a method for determining the bearing capacity for bridges based on plastic upper bound theory is described. Lastly a parameter study will be performed to show how changes in some of the parameters, included in the bearing capacity model, affect the bearing capacity.

In this chapter characteristic values, indicated by the subscript k , for strengths and loads are included in the equations. In following chapters these are substituted for design values or stochastic values.

5.1 Yield moment of cross section

Plasticity theory requires that the cross section should be balanced, which means that the reinforcement yields while failure happens in the concrete. For this to happen the ductility of the reinforcement steel has to be sufficient. This is assumed for this project.

The calculation of the yield moment, m_{yk} , is based on the compressive stress strain curve for concrete. Firstly DS/EN 1992-1-1 gives the parabolic-rectangular stress strain curve, which is illustrated in Figure 5.1. This stress strain can be simplified into a bilinear stress strain curve, which can be seen in Figure 5.2.

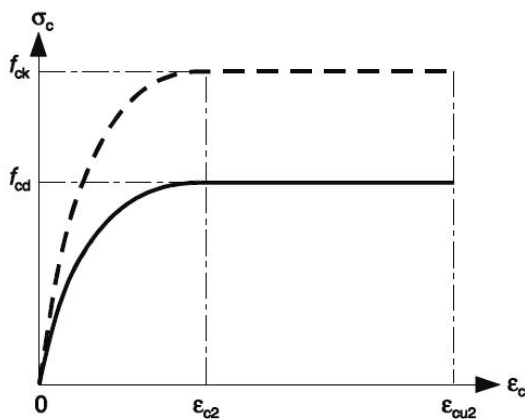


Figure 5.1: Compressive parabolic-rectangular stress strain curve for concrete. [Jensen, 2012]

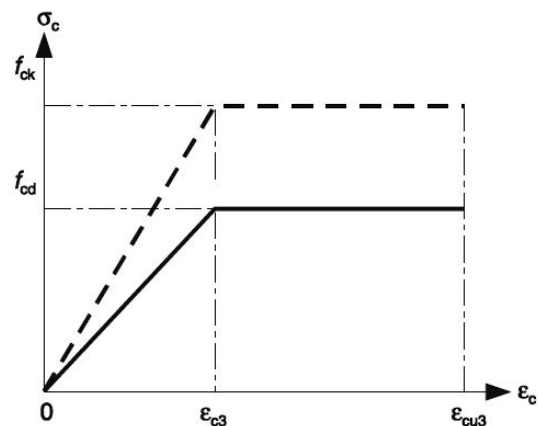


Figure 5.2: Compressive bilinear stress strain curve for concrete. [Jensen, 2012]

In DS/EN 1992-1-1 a further simplification of the bilinear stress strain curve is given as a rectangular stress strain curve, neglecting the first part of the bilinear stress strain curve. Then this rectangular stress strain curve is used to determine the yielding moment, for a cross section where the reinforcement yields and the concrete reaches failure, see Figure 5.3. This corresponds to a balanced cross section. In the figure, ε_{cu3} indicates the ultimate compressive strain, f_{ck} indicates the characteristic compressive yield strength of concrete and f_{yk} indicates the characteristic tensile yield strength of the reinforcement.

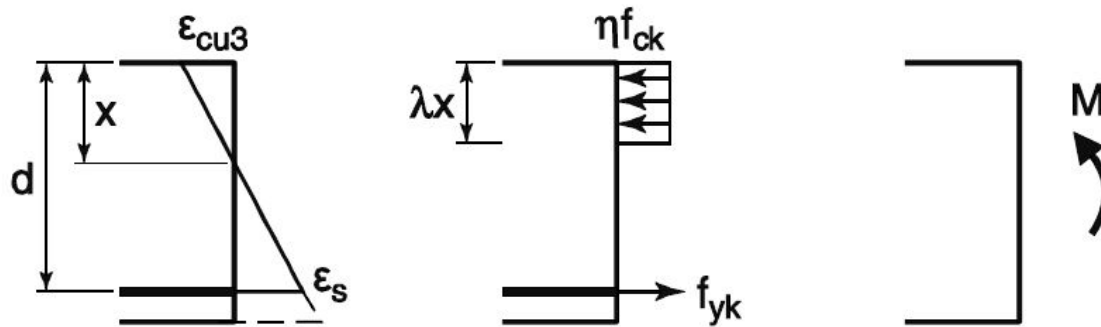


Figure 5.3: Cross section at plastic failure. [Jensen, 2012]

This report only takes into account bending moment. Therefore the tensile forces and compressive forces must be in equilibrium, which gives (5.1).

$$\eta f_{ck} \lambda x = A_s f_{yk} \quad (5.1)$$

Where:

η	Factor, see Figure 5.3. $\eta = 1$ for concrete grade C12-C50 [Jensen, 2012].
λ	Factor, see Figure 5.3. $\lambda = 0.8$ for concrete grade C12-C50 [Jensen, 2012].
x	Height of area in compression
A_s	Reinforcement area pr unit width
f_{ck}	Characteristic compressive yield strength of concrete
f_{yk}	Characteristic tensile yield strength of reinforcement steel

The reinforcement ratio is introduced as (5.2).

$$\omega = \frac{A_s f_{yk}}{d \eta f_{ck}} \quad (5.2)$$

Where:

ω	Reinforcement ratio
d	Distance from reinforcement to top, see Figure 5.3

From Figure 5.3, x can be calculated by (5.3).

$$x = \frac{\omega d}{\lambda} \quad (5.3)$$

The moment is determined at the reinforcement, which gives the yield moment pr unit width, m_{yk} , as (5.4).

$$m_{yk} = \left(d - \frac{\lambda x}{2}\right) \lambda x \eta f_{ck} \quad (5.4)$$

By substituting (5.3) into (5.4), (5.5) is found for the yield moment.

$$m_{yk} = \left(1 - \frac{\omega}{2}\right) \omega d^2 \eta f_{ck} \quad (5.5)$$

5.2 Application of upper bound slab theory for bridges

Upper bound theory states: "The load, which is found from the principle of virtual work for an arbitrary geometric failure mechanism, is larger than or equal to the yield load of the body". [Jensen and Bonnerup, 2014]

Therefore the aim is to set up different kinematically admissible failure mechanisms and find the failure mechanism giving the smallest bearing capacity and therefore the one closest to the exact bearing capacity for the specific case.

As will be described in a later chapter, the reliability method used in this project is Monte Carlo simulation, which is very time demanding. Therefore in order to save time it is chosen to determine the bearing capacity analytically from general failure mechanisms, rather than numerical FEM calculations. In Chapter 6 the analytical results are compared to numerical results of a FEM-software. Figure 5.4 illustrates the general failure mechanisms evaluated in this project. The circles in the figure indicate point loads from standard vehicle A.

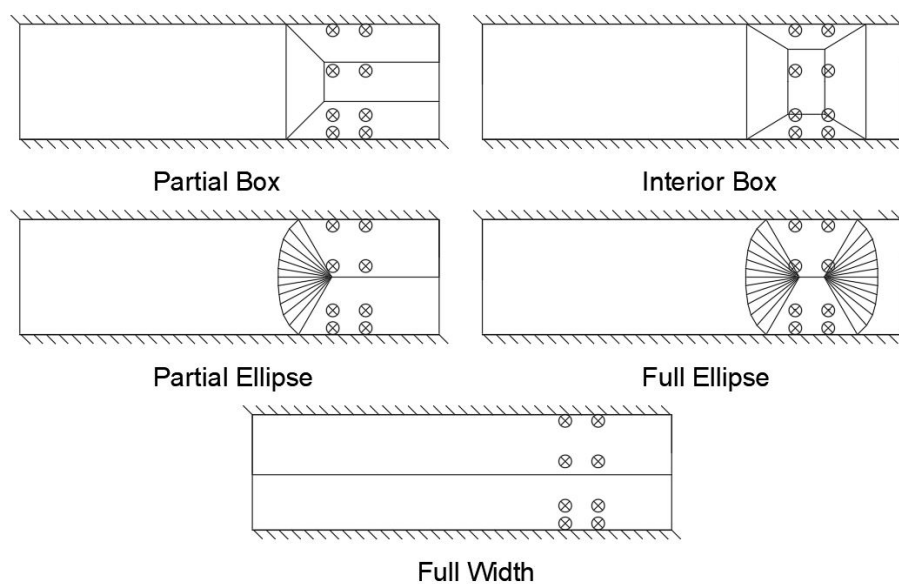


Figure 5.4: General failure mechanisms indicated by the yield lines evaluated.

No lengths are shown for the yield lines in Figure 5.4. The figure shows the general outline for the failure mechanisms. The calculated bearing capacity is of course dependent on the length of the yield lines. Therefore in order to get the bearing capacity value closest to the exact value, the failure mechanisms with different lengths of yield lines should be investigated. In order to find the lowest value of the bearing capacity a vector, a , is created containing a number of different failure mechanisms. The application of this vector is shown later in this chapter.

The bearing capacity will be determined as a factor C giving the relation between the considered traffic load value, Q_k , and the needed traffic load value for failure. Then $C \leq 1$ results in yielding of the structure, and the reliability can be determined on account of the axle configurations for specific standard vehicle classes.

C is determined from the principle of virtual work. The inner and outer work for any particular failure mechanism can be determined by (5.6) and (5.7), respectively

$$W_i = \sum_{j=1}^{N_y} m_{yk,j} \theta_j l_j \quad (5.6)$$

where:

W_i	Inner work
N_y	Number of yield lines
θ_j	Virtual rotation of yield line with index j
$m_{yk,j}$	Characteristic yield moment per unit length of yield line with index j
l_j	Length of yield line with index j

$$W_o = \int \int_A G_k(x,y) \delta(x,y) dx dy + C \sum_{i=1}^{N_F} Q_k c_{F,i} \delta_i \quad (5.7)$$

where:

W_o	Outer work
A	Displaced area of slab
G_k	Characteristic permanent load
δ	Virtual displacement
C	Bearing capacity given as a factor multiplication factor on the traffic load needed for failure
N_F	Number of wheels
Q_k	Characteristic traffic load
$c_{F,i}$	Percentage of vehicles weight on i 'th wheel
δ_i	Virtual displacement of i 'th wheel

By setting $W_i = W_o$, C can be determined for any particular failure mechanism. This is determined for each failure mechanism contained in the vector a , and the calculated C -value closest to the exact value, will be the smallest value. The expression for the C -value closest to the exact value is given in (B.1)

$$C = \min_a \left[\frac{\sum_{j=1}^{N_y} (m_{yk}(f_{yk}, f_{ck}))_j l_j \theta_j - \int \int_A G_k \delta(x, y) dx dy}{\sum_{i=1}^{N_F} Q_k c_{F,i} \delta_i} \right] \quad (5.8)$$

In Appendix B an example of the calculation of the bearing capacity for a specific case with a specific failure mechanism is presented.

All five of the general failure mechanisms should be considered when determining C , since each of them can be critical depending on geometry, reinforcement arrangement, position of standard vehicle A etc. This will be shown in the following section.

5.3 Parameter study

For the parameter study a base case is chosen for calculation of C , and then parameters such as permanent load and positioning of the traffic load, will be changed to show the effect on C of these changes. The base case will be Østerå bridge loaded by a class 200 standard vehicle in the normal passage situation. For this base case the characteristic loads and strength parameters, described in Chapter 3 and 4 are used. Figure 5.5 illustrates the static system for Østerå bridge, along with cross sections. Loads and strength parameters for the base case is given in Table 5.1.

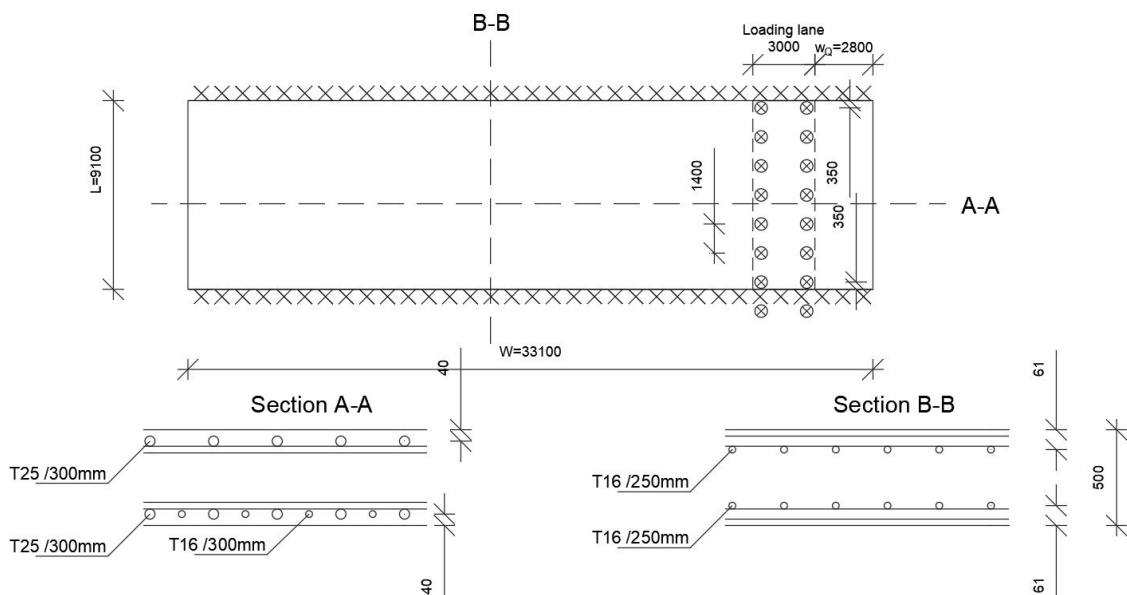


Figure 5.5: Base case. All dimensions are in [mm].

Table 5.1: Material parameters and loads for base case.

Parameter		Value
Reinforcement yield strength	f_{yk}	550 MPa
Concrete strength	f_{ck}	20 MPa
Traffic load	Q_k	2.58 MN
Permanent load	G_k	35.6 kN/m ²

C is calculated for the base case using the five previously mentioned failure mechanisms. Figure 5.6 to 5.10 illustrates the effect on C of changing different parameters used in the base case. Figure 5.6 shows the effect of change in reinforcement yield stress, Figure 5.7 shows the effect of change in dead load, Figure 5.8 shows the effect of change in slab width, Figure 5.9 shows the effect of placement of the standard vehicle in regards to the edge and 5.10 shows the effect of change in the span.

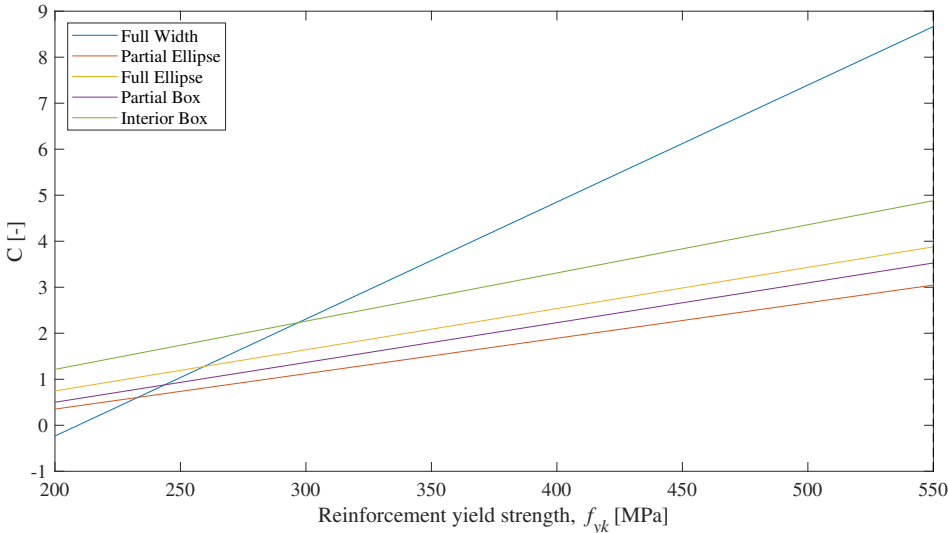


Figure 5.6: Effect on C of changing the yield strength of reinforcement, which for the base case was 550 MPa.

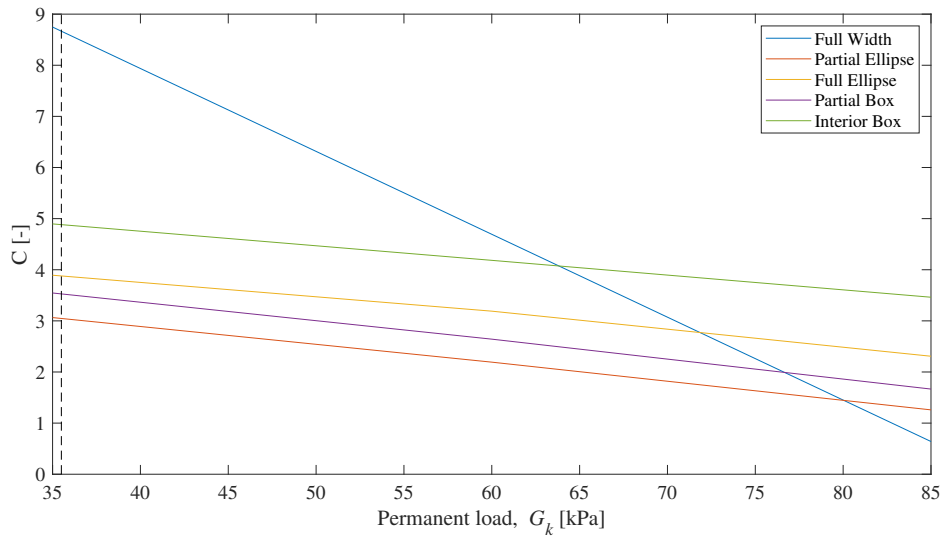


Figure 5.7: Effect on C of changing the dead load, which for the base case was 35.6 kN.

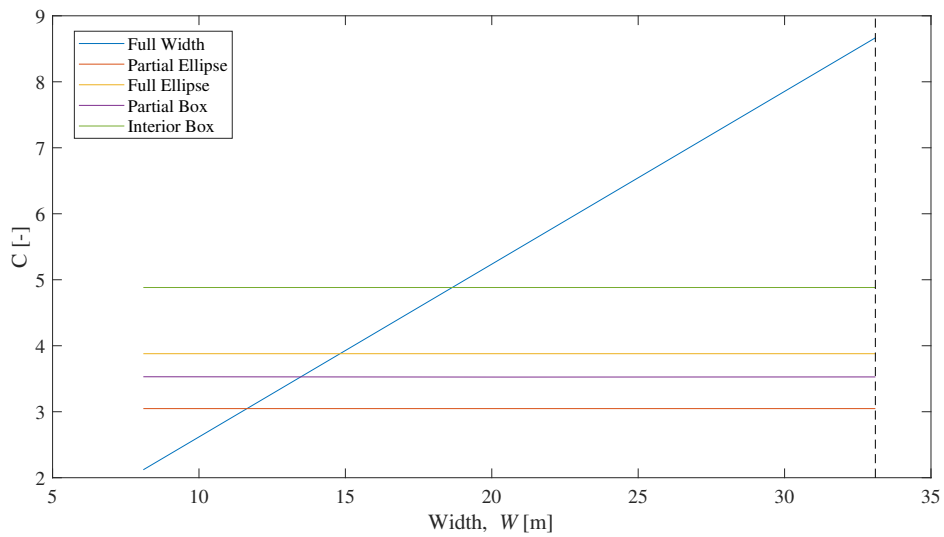


Figure 5.8: Effect on C of changing the width, which for the base case was 33.1 m

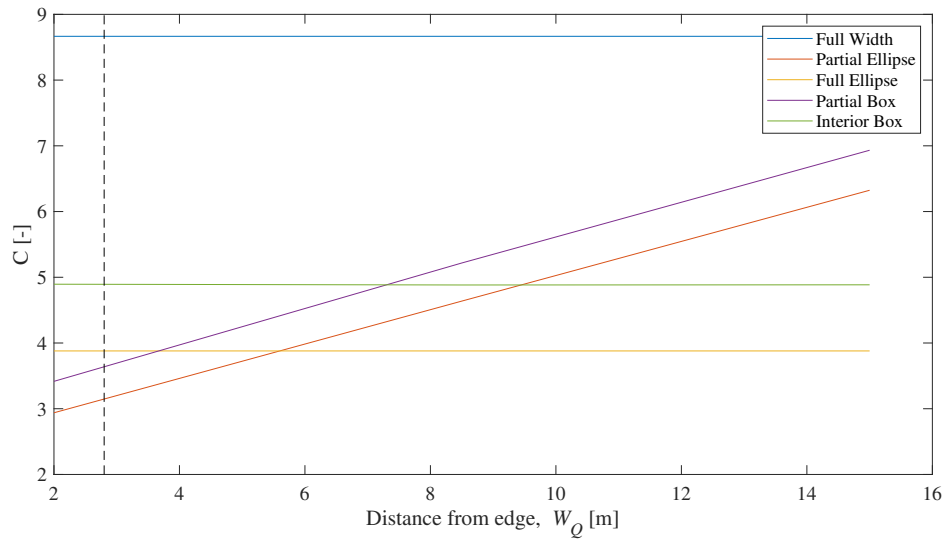


Figure 5.9: Effect on C of changing the distance of the vehicle to the edge, which for the base case was 5.4 m

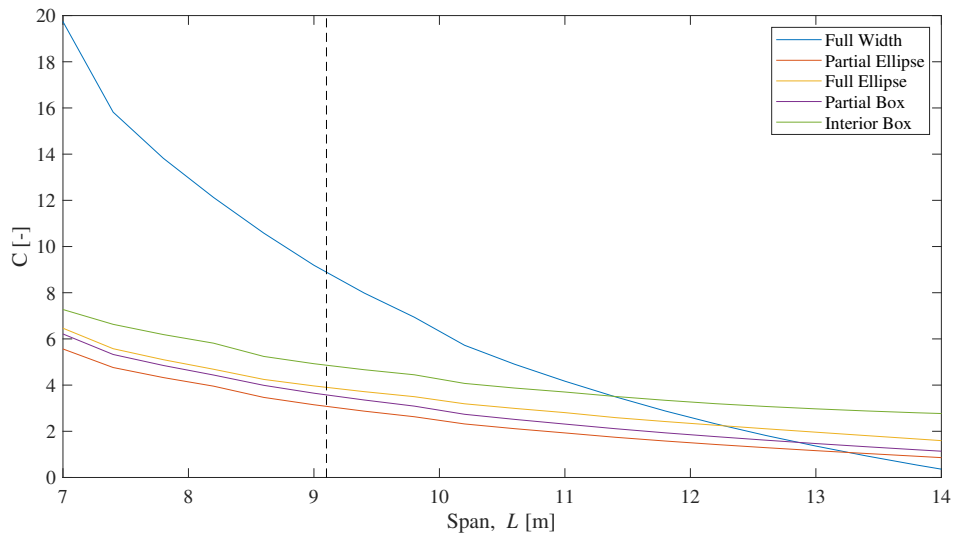


Figure 5.10: Effect on C of changing the span of the bridge which for the base case was 9.1 m

As can be seen from Figure 5.8, for the base case "Partial Ellipse" is the critical failure mechanism. But as the width becomes smaller and the ratio between width and span becomes more similar to that of long-span bridges, the "Full Width" failure mechanism becomes critical. Furthermore it can be seen that as the span increases C decreases for all failure mechanisms, which is to be expected.

Figure 5.9 shows that as the distance to the edge increases, C determined with "Partial Ellipse" is also increasing, and the "Full Ellipse" becomes critical at a certain distance.

As can be seen from Figure 5.7 and 5.6 the "Full Width" failure mechanism becomes critical with both decreasing yield stress of reinforcement and increasing dead load. Furthermore it can be seen that the slope of the "Full Width" failure mechanism is steeper than for the other failure mechanisms.

From the steepness of the lines in figure 5.6 and 5.7 it can be seen that a change in reinforcement strength and permanent load has larger effect on C for some failure mechanisms than for others. It can be seen that for the failure mechanism "Full width" the steepness is large compared to other failure mechanisms. This might mean that in the reliability assessment the standard deviation of C will differ depending on the failure mechanism. Figure 5.8, 5.9 and 5.10, show that the geometry of the bridge and positioning of standard vehicle A, affects which failure mechanism is critical. Therefore in Chapter 9, which describes the reliability analysis, as a sensitivity measure, changes will be made to the geometry of the bridge and the positioning of standard vehicle.

From looking at Figure 5.6 to 5.10 it can be seen that the failure mechanisms "Partial Box" and "Interior Box" are not critical in any shown cases. Therefore these won't be investigated further in this report.

6. Quantification of model uncertainty

When updating the reliability of existing bridges, there are some uncertainties, which should be taken into account. The uncertainties can be divided into the following groups:

- Physical uncertainty: The natural randomness of a quantity such as yield strength or the weight of a standard vehicle in a certain class.
- Measurement uncertainty: Uncertainty caused by imperfect measurements.
- Statistical uncertainty: Uncertainty due to limited sample size.
- Model uncertainty: Uncertainty related to imperfect knowledge or idealizations of the mathematical model.

The physical uncertainty will be taken into account by modelling the basic variables as stochastic variables corresponding to different distribution functions with some mean and variance, as described in Chapter 8. The statistical uncertainties can be reduced by increasing the sample size and the measurement uncertainties can be reduced by using better methods and tools of measurement.

In this chapter the model uncertainty of the bearing capacity model, described in Chapter 5, will be quantified by using the method from Annex D in [DS/EN-1990, 2007]. The standard procedure for evaluation of the resistance model described in Annex D of [DS/EN-1990, 2007] gives a mean correction factor or bias, b , for the model, and a corresponding coefficient of variation determined from the comparison of the resistance model results to experimental results. However experiments aren't carried out in this project, nor are results from previously carried out experiments used. Instead of carrying out experiments as prescribed by [DS/EN-1990, 2007] the results from the bearing capacity model will be compared to the results of the FEM program, Optum MP [Optum, 2020]. Optum MP is a relatively newly developed program, which calculate the moment bearing capacity of slabs using both upper and lower bound theories. However this introduces yet another model uncertainty as the results from Optum MP might not correspond perfectly with practical results. This model uncertainty is not included in the results shown below, but should be accounted for in applications on real bridges.

Some uncertainties aren't taken into account, such as the uncertainty in reinforcement grade of the reinforcements used. The bearing capacity assessments in this project are based on the static calculation documents. The position, size and grade of reinforcement might differ in practice from design. This uncertainty can be reduced by taking samples at the site of the existing bridge.

In the following section the computation model uncertainty will be quantified from the standard procedure in [DS/EN-1990, 2007].

6.1 Model uncertainty from the standard procedure in [DS/EN-1990, 2007]

The computation model uncertainty will be taken into account by using the following model:

$$C = b \Delta C_t(\mathbf{X}) \quad (6.1)$$

C_t	Bearing capacity from mathematical model as factor on traffic load for failure, see Chapter 5
b	Mean correction factor for the model, bias
Δ	Model Uncertainty: $\text{LN}(1, \sigma_\Delta)$
C	Bearing capacity including uncertainty on computational model
\mathbf{X}	Physical uncertainties - stochastic variables

The standard procedure is a method of determining b and σ_Δ . For this a sample of 54 slabs with different geometries, load cases and material strengths are investigated. A description of each case and the calculated bearing capacity from both Optum MP and the analytic model described in Chapter 5, are shown in Appendix C. The results are also illustrated in Figure 6.1, which also shows which failure mechanism was found to be critical by the analytic model. C_e indicates the result found from Optum MP and C_t indicates the result found from the analytic model.

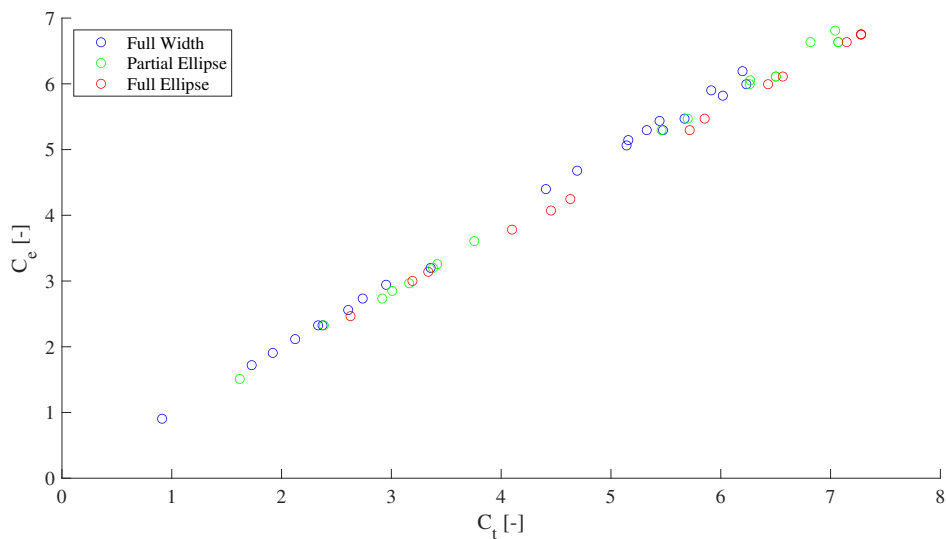


Figure 6.1: Comparison between Optum MP results and results from the model described in Chapter 5.

The bias is found by the least squares method by (6.2).

$$b = \frac{\sum_{i=1}^N C_e(\mathbf{x}_i) C_t(\mathbf{x}_i)}{\sum_{i=1}^N C_t(\mathbf{x}_i)^2} \quad (6.2)$$

The error term for each calculated case, Δ_i , is calculated by (6.3).

$$\Delta_i = \ln\left(\frac{C_e(\mathbf{x}_i)}{b C_t(\mathbf{x}_i)}\right) \quad (6.3)$$

The mean of the error terms $\bar{\Delta}$ is calculated by (6.4).

$$\bar{\Delta} = \frac{1}{N} \sum_{i=1}^N \Delta_i \quad (6.4)$$

The estimated value of the standard deviation, s_{Δ} , is calculated by (6.5).

$$s_{\Delta} = \sqrt{\frac{1}{N-1} \sum_{i=1}^N (\Delta_i - \bar{\Delta})^2} \quad (6.5)$$

The estimated value of the coefficient of variation, V_{Δ} is calculated by (6.6).

$$V_{\Delta} = \sqrt{\exp(s_{\Delta}^2) - 1} \quad (6.6)$$

This procedure has been used to determine the model uncertainty for both all failure mechanisms combined and each failure mechanism individually. The results are presented in Table 6.1 and the biases are illustrated in Figure 6.2 and 6.3.

Table 6.1: Computational model uncertainty parameters.

Failure mechanism	Bias. b [-]	Coefficient of variation, V_{Δ} [%]
Combined	0.95	2.8
Full Width	0.98	1.5
Partial Ellipse	0.95	1.5
Full Ellipse	0.93	0.9

As Table 6.1 shows, $b < 1$ for any failure mechanism. This is of course as expected since $b > 1$ would not be possible according to plastic upper bound theory if Optum is assumed to give the exact result.

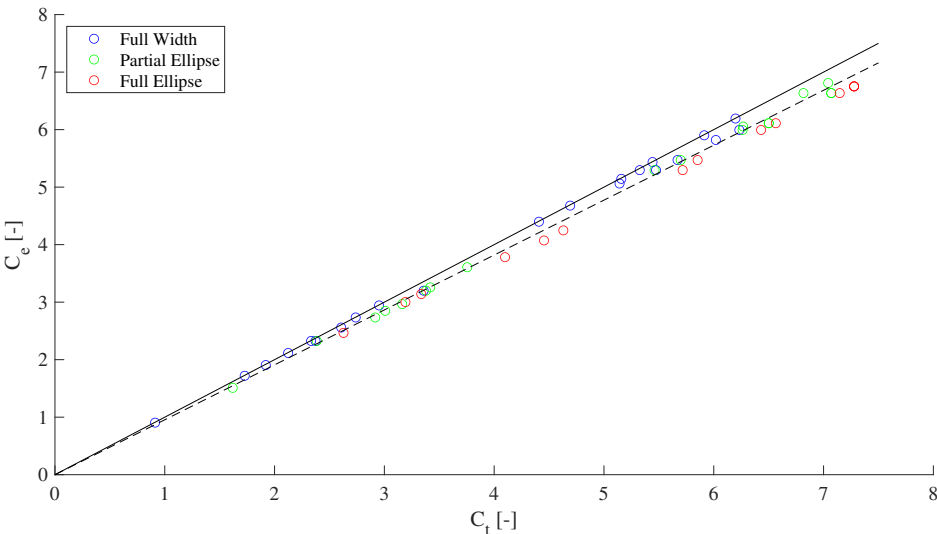


Figure 6.2: bias, b , for all failure mechanisms combined. The full line shows a bias, $b = 1$, and the dashed line shows the calculated bias.

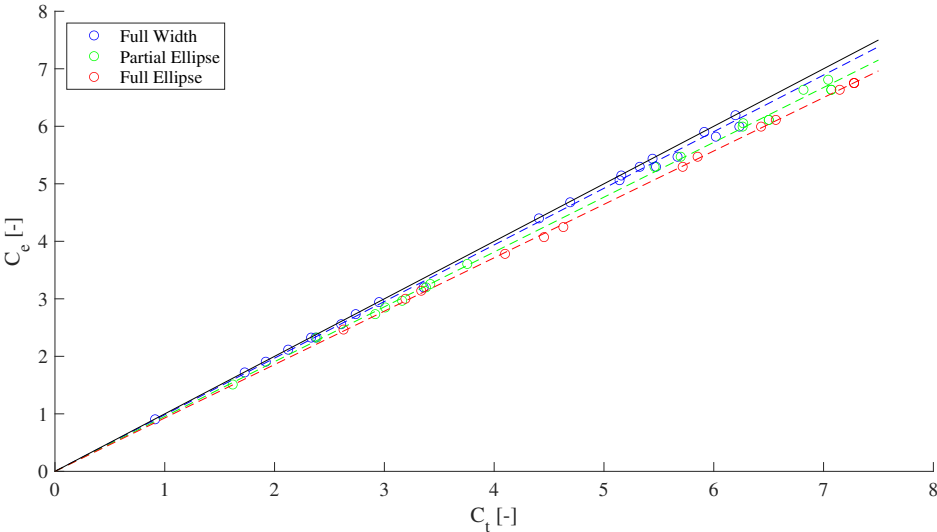


Figure 6.3: bias, b , for each failure mechanism. The full line shows a bias, $b = 1$, and the dashed line shows the calculated biases.

7. Deterministic analysis

As the bearing capacity model has been described, and as the bias of the model has been determined, the updated bearing capacity model can be used for bearing capacity assessment. The bearing capacity assessment can be performed by partial safety factor method through deterministic analysis with design values for material strengths and loads. As described in Chapter 5, the bearing capacity, C , is given as a multiplication on the traffic load needed for failure. The design value of C is determined by (7.1), which corresponds to EN1990: STR (6.10a). Notice the multiplication of the bias, b , which is found in Chapter 6. The static system is based on bridge dimensions, reinforcement and material strength as described in Chapter 3, and loading as described in Chapter 4.

$$C = \min_a \left[\frac{\sum_{j=1}^{N_y} (m_y (f_{y,k} / \gamma_{Ms}, f_{c,k} / \gamma_{Mc}))_j l_j \theta_j - \int \int_A G_k \gamma_G \delta(x, y) dx dy}{\sum_{i=1}^{N_F} Q_k \gamma_Q c_{F,i} \delta_i} \right] b \quad (7.1)$$

The deterministic analysis using the bearing capacity model from chapter 5 will be compared to a more traditional bearing capacity model not taking into account the transverse reinforcement. It is assumed that the traditional way to calculate the bearing capacity of a bridge is to divide the slab into a series of 3.5 m wide beams and using beam theory on the most unfavourably loaded beam. The beams are 3.5 m since this is assumed as the distribution width for the traffic load. The plastic upper bound solution for beams is calculated the same as for the "Full Width" failure mechanism for upper bound slab solution. This means that (7.1), is also used for the traditionally calculated C , but with a 3.5 m wide beam instead of the whole slab. The principle is illustrated in Figure 7.1a. For comparison figure 7.1b shows the failure mechanism, "Partial Ellipse", which was found to be critical for Østerå Bridge using the upper bound bearing capacity model. The upper bound slab model might give higher bearing capacity due to the higher number of yield lines, which means that the inner work is larger compared to the traditional model.

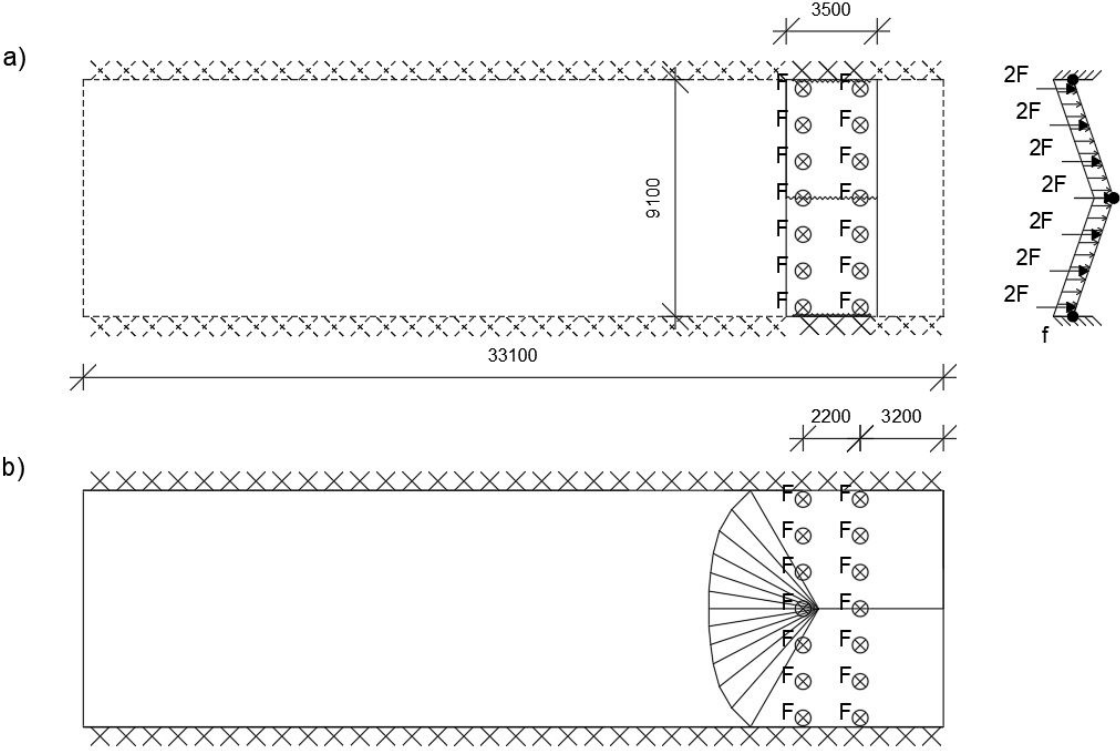


Figure 7.1: Principle for assumed traditional bearing capacity model and failure mechanism.

For the normal passage situation, the determined C-values for both the upper bound model and for the traditional model, are given in Table 7.1.

Table 7.1: C found from deterministic analysis for normal passage.

Vehicle class	Traditional model	Model from Chapter 5
100	1.02	2.80
125	0.86	2.30
150	0.80	2.14
175	0.73	1.95
200	0.69	1.85

As can be seen from Table 7.1, using the traditional model, Østerå Bridge can be classified for class 100 vehicles. This corresponds to the current classification of the bridge in normal passage. However as the bridge is investigated only using standard vehicle A, the "traditional model" might be conservative. But as the allowable vehicle class, which is found with this model, is the same as what is given by the Road Directorate, this model will be considered adequate for comparison with the upper bound model from Chapter 5.

Table 7.1 shows that using the model from Chapter 5, Østerå Bridge can be classified for class 200 vehicles, which is the highest vehicle class investigated in this project. Moreover, it can be seen that using the upper bound model, more than 2 class 100 vehicles, which the bridge is classified for, could be stacked on top of each other without failure.

8. Stochastic modelling

For the reliability-based bearing capacity assessment, and for determination of a proof load factor, taking into account the resistance, stochastic models used to model the different uncertainties described in Chapter 6. Three general stochastic models are investigated, the stochastic model given by the danish road directorate in [Vejdirektoratet, 2004], the stochastic model, which is the basis for the bridge specific national annex to Eurocodes 1990 and 1991, given in [Sørensen, 2009] and the stochastic model in [Sørensen, 2016]. The stochastic model in [Sørensen, 2016] is the same as that in [Sørensen, 2009], but with a revised dynamic factor. The stochastic model from [Sørensen, 2009] and [Sørensen, 2016] will be investigated using the model uncertainty on the computational model described in Chapter 6. The stochastic model given by [Vejdirektoratet, 2004] already includes a model uncertainty on the computation model. Therefore the stochastic model from [Vejdirektoratet, 2004] will be investigated with both the uncertainty model already included and the uncertainty model found in Chapter 6. This gives a total of four stochastic models to be investigated, which can be seen from Table 8.1.

Table 8.1: Stochastic models investigated in this report.

Stochastic model	General stochastic model	Model uncertainty on Computational model
1	[Sørensen, 2009]	Chapter 6
2	[Sørensen, 2016]	Chapter 6
3	[Vejdirektoratet, 2004]	[Vejdirektoratet, 2004]
4	[Vejdirektoratet, 2004]	Chapter 6

The stochastic models will be described further in the following, and differences in the stochastic models will be illustrated by distribution figures. Finally the stochastic models will be summed up in the end of this chapter.

8.1 Load model

In the scope of this project only traffic loads and self weights are considered, since loads such as wind loads, snow loads etc. are assumed negligible for short span bridges.

8.1.1 Permanent load

The permanent load, G , is the self weight of the structure, which is modelled as a normally distributed variable with a coefficient of variation $V_G = 5\%$ in [Vejdirektoratet, 2004] and $V_G = 10\%$ in [Sørensen, 2009]. The stochastic model of [Sørensen, 2009] is for design of

new bridges. For existing structures it can be argued that there is better knowledge on the permanent load, and therefore $V_G = 5\%$ is instead used for stochastic model 1 and 2.

A model uncertainty in connection with the permanent load is also introduced in [Vejdirektoratet, 2004]. This is done by addition of I_G to G . I_G has mean value, $\mu_{I_G} = 0$ and a standard deviation, σ_{I_G} , equal to the standard deviation of the permanent load, σ_G .

Figure 8.1 shows the distribution of the permanent load with corresponding model uncertainty for the four stochastic models. In stochastic model 1 and 2, there is no model uncertainty on the permanent load included.

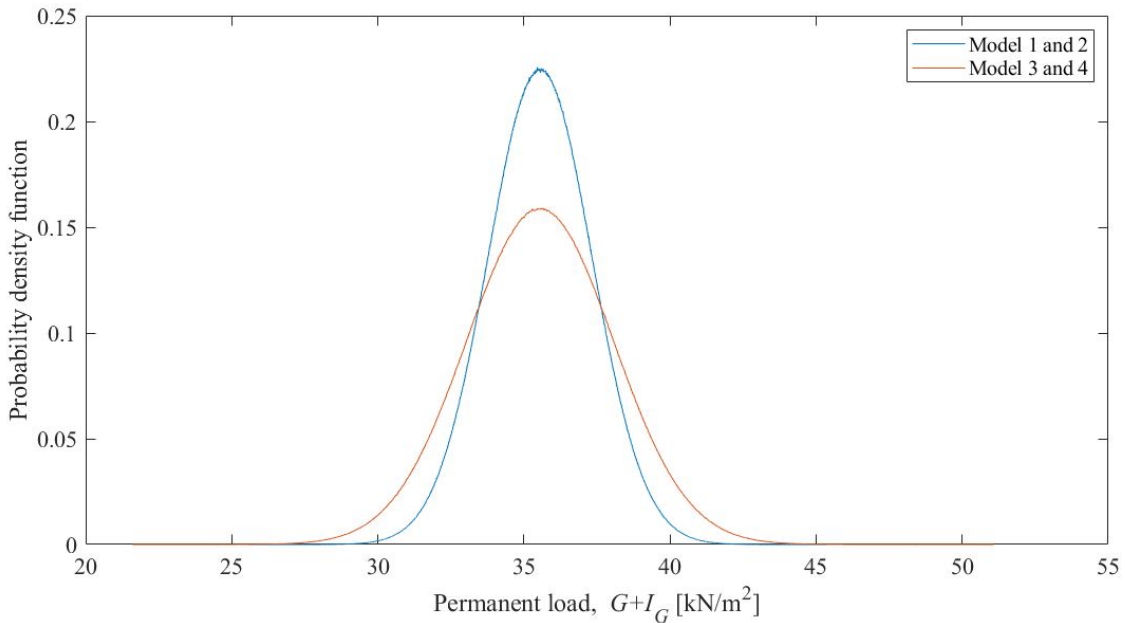


Figure 8.1: Permanent load distribution for the stochastic models.

As can be seen from Figure 8.1 the standard deviation is larger for stochastic model 3 and 4 than for stochastic mode 1 and 2. This is of course as expected since V_G is the same for all models, but model 1 and 2 include a model uncertainty.

8.1.2 Traffic load

The annual extreme traffic load is found as (8.1).

$$Q = PK_s \tag{8.1}$$

Where:

Q		Annual extreme traffic load
P		Annual extreme vehicle weight
K_s		Dynamic factor

The distribution for the annual extreme vehicle weight is the same for all stochastic models and is described in Chapter 4.

Dynamic effects

Dynamic effects during normal passage from vehicles on the bridge are modelled by multiplying the static load with a dynamic factor, K_s . This is given by (8.2).

$$K_s = (1 + S_t) \quad (8.2)$$

Where S_t is the dynamic supplement, which for global effects is normally distributed with $N(41.5/W, 41.5/W)$ in both [Vejdirektoratet, 2004] and [Sørensen, 2009]. W is the weight of the vehicle in kN. As mentioned earlier the dynamic factor model found in [Sørensen, 2016] will also be investigated. This found that a stochastic model with $K_s = N(1.02, 0.00128)$ will give sufficient reliability for bridges.

Model uncertainty

In [Vejdirektoratet, 2004] the model uncertainty of the variable load is included by the normally distributed stochastic variable, I_Q , which has a mean value, $\mu_{I_Q} = 1.0$ and coefficient of variation, V_{I_Q} as given in Table 8.2.

Table 8.2: Coefficient of variation for I_Q . [Vejdirektoratet, 2004]

Uncertainty in loading model	Low	Medium	High
V_{I_Q}	0.10	0.15	0.20

V_{I_Q} can as a starting point be taken as low for conditional passage and for the normal passage situations in which the relative influence of the ordinary traffic on safety is minor [Vejdirektoratet, 2004]. This is assumed for the cases in this report.

In [Sørensen, 2009] I_Q is lognormally distributed with $\mu_{I_Q} = 1.0$ and $V_{I_Q} = 0.1$.

Figure 8.2 shows the distribution of the traffic load for a class 200 standard vehicle with corresponding model uncertainty for the four stochastic models.

Figure 8.2 shows that there seems to be little difference in the traffic load models for the four stochastic models.

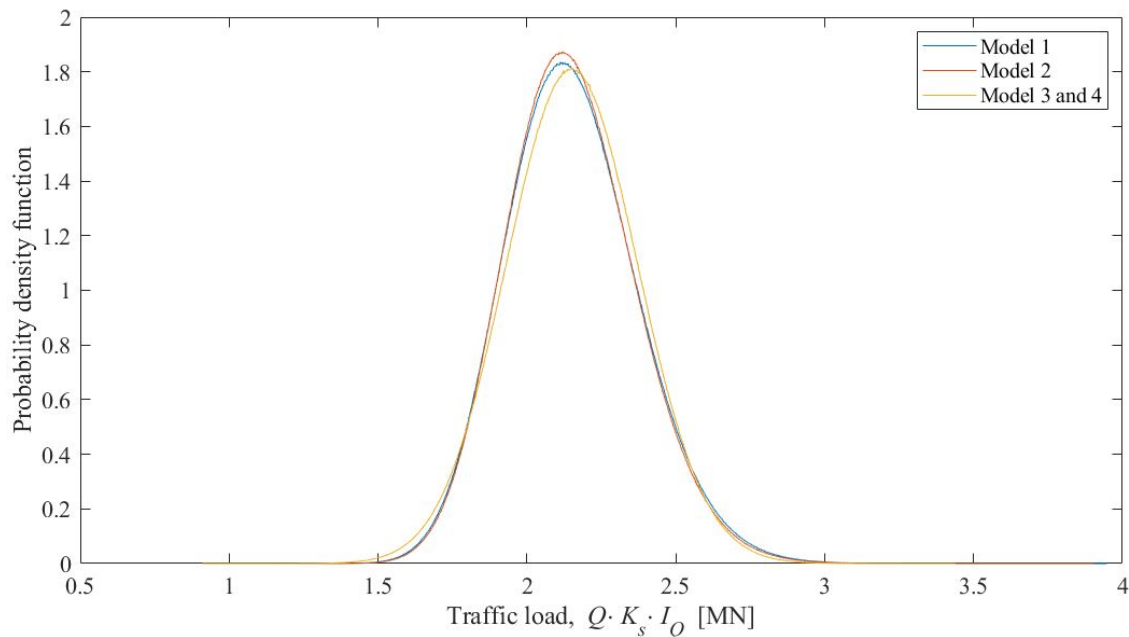


Figure 8.2: Traffic load distribution for the stochastic models.

8.2 Material model

The materials used are concrete and reinforcement steel.

8.2.1 Reinforcement steel

In [Vejdirektoratet, 2004] the yield stress of non-prestressed reinforcement is assumed lognormally distributed with stochastic parameters as shown in Table 3.2. Østerå bridge is reinforced by Tentor steel.

In [Sørensen, 2009] the yield stress of reinforcement is lognormally distributed. For the stochastic models based on [Sørensen, 2009], the mean from Table 3.2 will be used along with a coefficient of variation of 7%

8.2.2 Concrete

In [Vejdirektoratet, 2004] the compressive strength of non-prestressed reinforcement is assumed lognormally distributed with stochastic parameters given in Table 3.3.

In [Sørensen, 2009] the concrete strength is lognormally distributed. For the stochastic models based on [Sørensen, 2009], the mean values for compressive concrete strength from Table 3.3 will be used along with coefficient of variation of 14%

8.2.3 Model uncertainty

For material parameters the model uncertainty is included by multiplying the basic strength parameters with the stochastic variable I_m . I_m is lognormally distributed with

mean value, $\mu_{I_m} = 1.0$. The coefficient of variation, V_{I_m} , in [Vejdirektoratet, 2004] is given by (8.3)

$$V_{I_m} = \sqrt{V_{I_1}^2 + V_{I_2}^2 + V_{I_3}^2 + 2(\rho_1 V_{I_1} + \rho_2 V_{I_2} + \rho_3 V_{I_3}) V_m} \quad (8.3)$$

Where:

V_{I_m}	COV for material model uncertainty.
V_m	Material coefficient of variation
V_{I_1}	COV for uncertainty for accuracy of computation model.
ρ_1	Correlation between V_{I_1} and V_m .
V_{I_2}	COV for model uncertainty for uncertainty in determination of material parameter for the structure on the basis of the vicarious material parameter
ρ_2	Correlation between V_{I_2} and V_m .
V_{I_3}	COV for model uncertainty for material identity.
ρ_3	Correlation between V_{I_3} and V_m .

The coefficient of variation, V_{I_i} , and correlation, ρ_i , for $i=1,2,3$ are given in the following Table 8.3.

Table 8.3: Coefficient of variation and correlation for I_i for $i=1,2,3$. [Vejdirektoratet, 2004]

	Good	Normal	Poor
V_{I_i}	0.04	0.06	0.09
ρ_i	-0.3	0.0	0.3

In stochastic model 4, the model uncertainty from Chapter 6 will be used. Therefore V_{I_1} and ρ_1 will not be included in the material model uncertainty for stochastic model 4.

[Vejdirektoratet, 2004] states: "Normal calculation accuracy is usually used in situations where computation models are used that are generally accepted as being in conformity with normal practice". As yield line theory is assumed normal practice for bearing capacity calculation for slabs, V_{I_1} and ρ_1 are based on normal uncertainty for stochastic model 3.

According to [Vejdirektoratet, 2004], V_{I_2} and ρ_2 are based on poor uncertainty for concrete and normal uncertainty for reinforcement in the preparation of DS 411. This will also be used in this project.

[Vejdirektoratet, 2004] states: "Normally material identity is assumed when the materials are assigned on the basis of the project material and there is no reason to doubt that the bridge in question was not built in accordance with the project material". This is assumed for Østerå bridge and therefore V_{I_3} and ρ_3 are based on normal uncertainty.

In [Sørensen, 2009] the material model uncertainty of $V_{I_m}=0.11$ and $V_m=0.05$ is used for concrete and reinforcement strength, respectively, along with the mean values given in Chapter 3.

Figure 8.3 shows the distribution of the reinforcement yield strength with corresponding model uncertainty, and Figure 8.3 shows the distribution of the concrete strength with corresponding model uncertainty, for the four stochastic models.

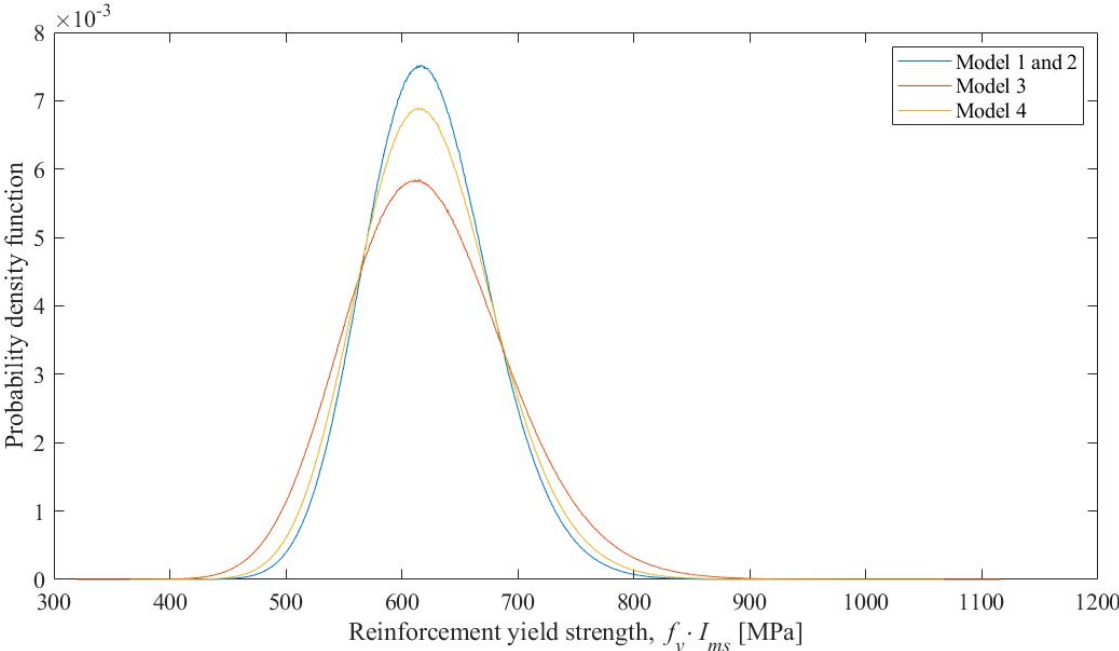


Figure 8.3: Reinforcement yield strength distribution for the stochastic models.

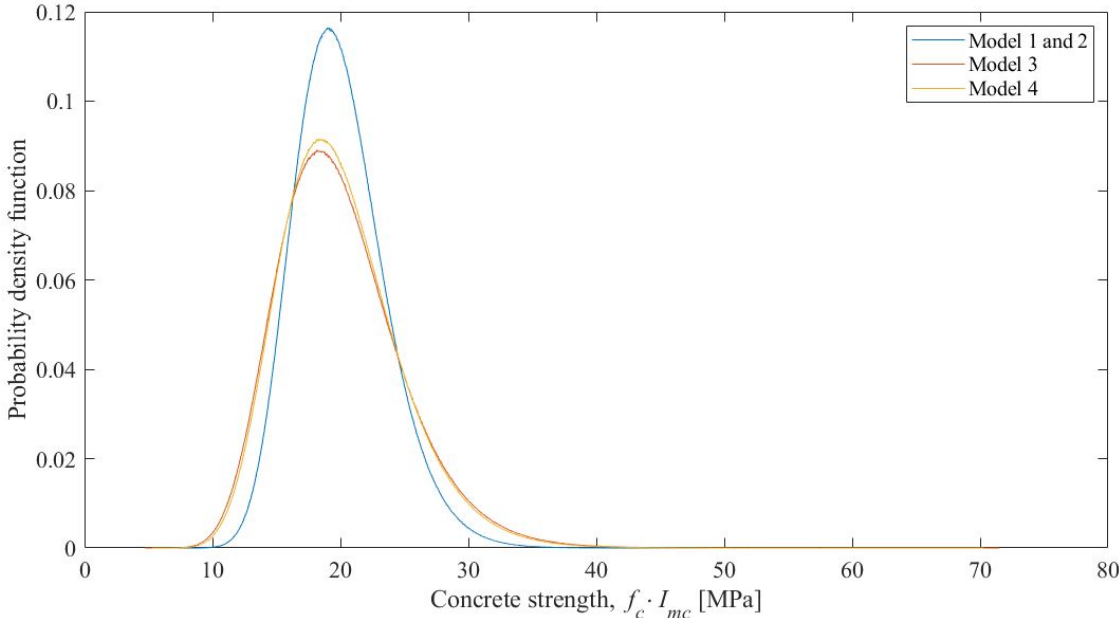


Figure 8.4: Concrete strength distribution for the stochastic models.

As can be seen from Figure 8.3 and 8.4 the standard deviation for the load parameters with corresponding model uncertainties is largest for model 3 and smallest for model 1 and 2.

8.3 Applied stochastic models

Based on Chapter 5 and 6 as well as what is described in this chapter a general limit state equation can be written as (8.4), where the yield moment and degree of reinforcement are calculated by (8.5) and (8.6), respectively.

$$g = \min_a \left[\frac{\sum_{j=1}^{N_y} (m_y(f_y, I_{ms}, f_c, I_{mc}))_j \theta_j l_j - \int \int_A (I_G + G) \delta(x, y) dx dy}{\sum_{i=1}^{N_F} I_Q (1 + S_t) P c_{F,i} \delta_i} \right] b \Delta - 1 \quad (8.4)$$

$$m_y(f_y, I_{ms}, f_c, I_{mc}) = \left(1 - \frac{\omega(f_y, I_{ms}, f_c, I_{mc})}{2}\right) \omega(f_y, I_{ms}, f_c, I_{mc}) d^2 \eta f_c I_{mc} \quad (8.5)$$

$$\omega(f_y, I_{ms}, f_c, I_{mc}) = \frac{A_s f_y I_{ms}}{d \eta f_c I_{mc}} \quad (8.6)$$

a	Vector containing different failure mechanisms, as described in Ct 5.
N_y	Number of yield lines
f_y	Yield strength of steel, stochastic
I_{ms}	Model uncertainty on yield strength of steel, stochastic
f_c	Compressive strength of concrete, stochastic
I_{mc}	Model uncertainty on compressive strength of concrete, stochastic
$m_{y,j}$	Yield moment at yield line with index j , stochastic as function of stochastic variables
θ_j	Virtual rotation at yield line with index j
l_j	Length of yield line with index j
A	Deflected area
G	Permanent load, Stochastic
I_G	Model uncertainty of permanent load, stochastic
P	Annual maximum vehicle weight, Stochastic
I_Q	Model uncertainty of traffic load,
S_t	Dynamic factor, stochastic
δ	Virtual deflection
N_F	Number of point loads
$c_{F,i}$	Percentage of extreme value traffic load on i 'th wheel
b	Bias of computation model
Δ	Model uncertainty of computation model, stochastic
A_s	Area of yielding reinforcement per unit length
ω	Degree of reinforcement
d	Distance from yielding reinforcement to edge of slab

The modelling described in the previous sections, gives the stochastic models in Table 8.4 for investigations in this report.

Table 8.4: Parameters for stochastic models investigated in this project.

Stochastic model		Distribution type	Mean	COV	Characteristic
Reinforcement strength					
1 and 2	f_y	Lognormal	623 MPa	7%	5% (554 MPa)
3 and 4	f_y	Lognormal	623 MPa	4%	550 MPa (0.1%)
Reinforcement strength model uncertainty					
1 and 2	I_{ms}	Lognormal	1	5 %	
3	I_{ms}	Lognormal	1	10.4 % ⁽¹⁾	
4	I_{ms}	Lognormal	1	8.5 % ⁽¹⁾	
Concrete strength					
1 and 2	f_c	Lognormal	20 MPa	14%	5% (15.8 MPa)
3 and 4	f_c	Lognormal	20 MPa	18%	5% (14.7 MPa)
Concrete strength model uncertainty					
1 and 2	I_{mc}	Lognormal	1	11 %	
3	I_{mc}	Lognormal	1	15.8 % ⁽¹⁾	
4	I_{mc}	Lognormal	1	14.6 % ⁽¹⁾	
Permanent load					
1 and 2	G	Normal	35.5 kN/m ²	10%	50 %
3 and 4	G	Normal	35.5 kN/m ²	5%	50 %
Permanent load model uncertainty					
1 and 2		Not included			
3 and 4	I_G	Normal	0	$\sigma_{I_G} = \sigma_G$ ⁽²⁾	
Annual maximum vehicle weight					
All	Q	See Ct 4			98 %
Annual maximum vehicle weight model uncertainty					
1 and 2	I_Q	Lognormal	1	10%	
3 and 4	I_Q	Normal	1	10%	
Vehicle weight					
All	W	Normal	See Ct 4	See Ct 4	
Dynamic factor					
1, 3 and 4	S_t	Normal	41.5/W (W in kN)	100 %	0.23 ⁽³⁾
2	(1+S _t)	Normal	1.02	0.125 %	1.23 ⁽³⁾
Bias					
All	b	Deterministic	See Ct 6		
Computation model uncertainty					
1, 2 and 4	Δ	Lognormal	1	See Ct 6	
3		Included in I_m			

⁽¹⁾ The difference in coefficient of variation value between model 3 and 4 is due to the inclusion of computational model uncertainty in I_m in model 3.

⁽²⁾ Since the mean value is 0, the coefficient of variation is undefined. Therefore this is instead given as the standard deviation.

⁽³⁾ This value is specifically found for the span of Østerå bridge of 9.1 m. See Chapter 4, to see how this changes for other spans.

9. Reliability analysis

An existing bridge can be up classified if it is shown that the annual reliability index, with the load model for the given vehicle class, is equal to or larger than the required annual reliability index. The required annual probability of failure was in Chapter 2 found to be $P_f = 10^{-6}$ for existing bridges in CC3, corresponding to an annual reliability index of $\beta = 4.8$

In this chapter the reliability method will first be specified and then the reliability analyses will be performed. Lastly a parameter study will be presented.

9.1 Reliability method

To assess the reliability using the presented bearing capacity model, it is chosen to use Monte-Carlo simulations over e.g. first-order and second-order reliability methods, due to the high degree of non-linearity associated with the model. As can be seen from Section 5.3, different values of the stochastic variables may cause different failure mechanisms to be critical. This can be taken into account through Monte-Carlo simulations, where the critical failure mechanism can be determined for each simulated set of realisations of the stochastic variables.

When performing Monte-Carlo simulations the uncertainty of the estimated reliability depends on the number of failures. In order to secure a sufficient confidence in the estimate there should be a sufficient number of simulations giving failure. This is secured by performing 100 times the reciprocal of the desired probability of failure. Therefore in order to secure a sufficient confidence for a probability of failure of $P_f = 10^{-6}$, 10^8 simulations are performed. This gives a standard deviation on the estimate of $s = 10^{-7}$ if $P_f = 10^{-6}$ as determined by (9.1). This corresponds to a coefficient of variation of 0.1.

$$s = \sqrt{\frac{P_f(1 - P_f)}{\text{number of simulations}}} \quad (9.1)$$

9.2 Reliability analysis

The limit state function for the bearing capacity model is written as (9.2).

$$g = \min_a \underbrace{\left[\frac{\sum_{j=1}^{N_y} (m_y(f_y, I_{f_y}, f_c, I_{f_c}))_j \theta_j - \int \int_A (I_G + G) \delta(x, y) dx dy}{\sum_{i=1}^{N_F} I_Q (1 + S_t) Q c_{F,i} \delta_i} \right]}_C b \Delta - 1 \quad (9.2)$$

Where:

a	Vector containing different failure mechanisms, as described in Ct 5.
N_y	Number of yield lines
f_y	Yield strength of steel, stochastic
I_{f_y}	Model uncertainty on yield strength of steel, stochastic
f_c	Compressive strength of concrete, stochastic
I_{f_c}	Model uncertainty on compressive strength of concrete, stochastic
$m_{y,j}$	Yield moment at yield line with index j , stochastic as function of stochastic variables
θ_j	Virtual rotation at yield line with index j
A	Deflected area
G	Permanent load, Stochastic
I_G	Model uncertainty of permanent load, stochastic
Q	Annual maximum traffic load, Stochastic
I_Q	Model uncertainty of traffic load,
S_t	Dynamic factor, stochastic
δ	Virtual deflection
N_F	Number of point loads
$c_{F,i}$	Percentage of extreme value traffic load on i 'th wheel
b	Bias of computation model
Δ	Model uncertainty of computation model, stochastic

When performing the simulations every set of realizations of stochastic variables giving $g \leq 0$ or $C \leq 1$ are stored as failures. As described in Chapter 5 C gives a factor multiplied to the realized traffic load, that would precisely give failure given the simulated set of realizations. This means that $C=1$ just gives failure for the realized case, and C -values lower also gives failure.

When 10^8 simulations are performed for Østerå Bridge with a class 200 standard vehicle and the stochastic models described in Chapter 8, no failures are realized. This means that solely based on the reliability-based bearing capacity assessment the bridge could be up-classified for allowance of class 200 standard vehicles. However it should be noted that this estimate is based on previously mentioned simplifications and limitations, such as the neglect of Standard Vehicle B and ordinary traffic in the load model.

In order to get some data for the parameter study and to compare the reliability-based analysis to a deterministic analysis, the variable z is introduced into (9.2), see (9.3).

$$g = \min_a \underbrace{\left[\frac{z \sum_{j=1}^{N_y} (m_y(f_y, I_{f_y}, f_c, I_{f_c}))_j \theta_j - \int \int_A (I_G + G) \delta(x, y) dx dy}{\sum_{i=1}^{N_F} I_Q (1 + S_t) Q c_{F,i} \delta_i} \right]}_C b \Delta - 1 \quad (9.3)$$

z is determined from the design equation, such that the resistance multiplied by z accurately gives failure i.e. design based on the partial safety factor approach. Based on the limit state equation (9.2) the design equations can be written as (9.4) and (9.5), which correspond to EN1990: STR (6.10a) and EN1990: STR (6.10b), respectively. z_a and z_b are found from these two equations and z is found as $z=\max[z_a, z_b]$.

$$\min_a \left[z_a \sum_{j=1}^{N_y} (m_y(f_{y,k} \gamma_{ms}, f_{c,k} \gamma_{mc}))_j \theta_j - \int \int_A G_k \gamma_{Ga} \delta(x,y) dx dy \right] b = 0 \quad (9.4)$$

$$\min_a \left[\frac{z_b \sum_{j=1}^{N_y} (m_y(f_{y,k} \gamma_{ms}, f_{c,k} \gamma_{mc}))_j \theta_j - \int \int_A G_k \gamma_{Gb} \delta(x,y) dx dy}{\sum_{i=1}^{N_F} Q_k \gamma_Q c_{F,i} (1 + S_t)_k \delta_i} \right] b = 1 \quad (9.5)$$

The value of the partial safety factors, which are included in (9.4) and (9.5) can be found in Table 2.1.

10^8 simulations of (9.3) have been performed for Østerå bridge using all 4 stochastic models with a class 200 standard vehicle. For stochastic model 3 the C -values for all realizations has been put into a histogram, which is shown in Figure 9.1. Furthermore the critical failure mechanism has been stored for each simulation. For description of the failure mechanisms see Figure 5.4.

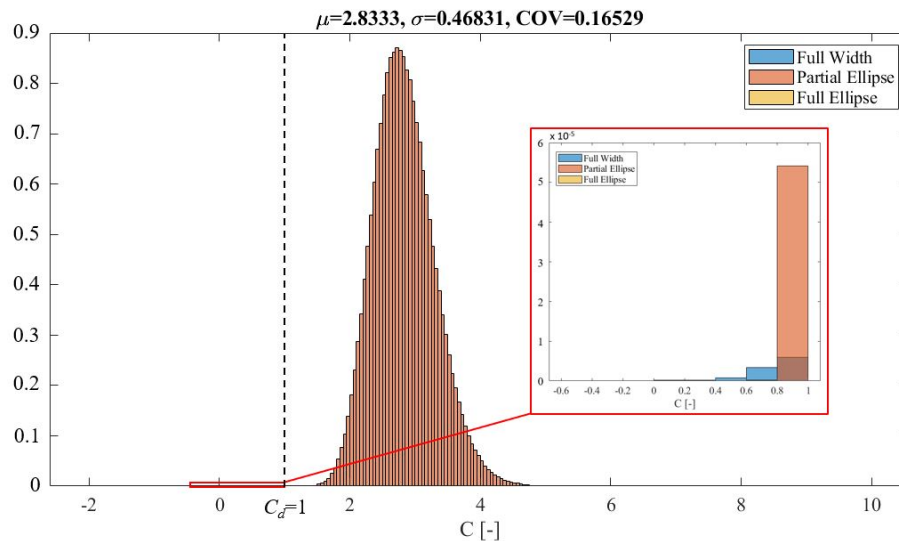


Figure 9.1: The distribution of the realized factor C for the stochastic model 1, normalized for probability density.

It can be seen from Figure 9.1, that for most of the simulations, the critical failure mechanism is "Partial Ellipse". However at the tail end, where $C \leq 1$, some of the simulations give "Full Width" as the critical failure mechanism. In the parameter study it will be shown how changes in geometry affects, which failure mechanisms are critical and in turn how this affects the reliability.

In Table 9.1 the results for all stochastic models are shown. In Table Table 9.1 some annual

probabilities of failure are lower than 10^{-6} . It should be noted that for these the coefficient of variation of the estimate is of course larger than 0.1.

Table 9.1: Results from simulations of (9.3).

Stochastic model	z	P_f	β
1	0.74	$0.02 \cdot 10^{-6}$	5.49
2	0.74	$0.02 \cdot 10^{-6}$	5.49
3	0.75	$3.25 \cdot 10^{-6}$	4.51
4	0.75	$0.10 \cdot 10^{-6}$	5.20

It can be seen from Table 9.1 that all but stochastic model 3 give an annual reliability lower than the required annual reliability. This could suggest that using the partial safety factor method would not give the desired reliability for stochastic model 3. Stochastic model 3 and 4 are based on the stochastic model of [Vejdirektoratet, 2004], which should be used for classification of existing bridges according to [Vejdirektoratet, 2017].

Table 9.1 shows no difference in the results for stochastic model 1 and 2. The only difference between these stochastic models is the dynamic factor. This suggests that the chosen dynamic factor model has little importance on the reliability. Furthermore the Table shows relatively large difference in the results between stochastic model 3 and 4. The difference here is that the model uncertainty on the bearing capacity model is multiplied to C for model 4 as described in Chapter 6. For model 3 the model uncertainty on the bearing capacity model is included in the material model uncertainties. This might suggest that the material model uncertainties has high importance for the reliability. The importance of the stochastic variables will be investigated further in the parameter study.

Simulations of (9.3) are also performed for the traditional bearing capacity model, which is described in Chapter 7, with a class 200 vehicle. The results can be seen in Table 9.2. If no failures are realized with 10^8 simulations, the annual probability of failure is just given as $< 0.01 \cdot 10^{-6}$

Table 9.2: Results from simulations of (9.2) with the traditional model.

Stochastic model	z	P_f	β
1	1.52	$< 0.01 \cdot 10^{-6}$	> 5.61
2	1.52	$< 0.01 \cdot 10^{-6}$	> 5.61
3	1.53	$0.08 \cdot 10^{-6}$	5.24
4	1.53	$< 0.01 \cdot 10^{-6}$	> 5.61

In Table 9.2 it is shown, that the annual probability of failure is lower than the required annual probability of failure for all stochastic models. This suggests that using the partial safety factor method for the traditional model gives sufficient reliability. The reliability index is also larger for the traditional bearing capacity model than what was found for the upper bound model in Table 9.1. However, as was found in Chapter 7, there is a lot to be gained from using the upper bound model, as Østerå bridge can be classified for class 125 vehicle using the traditional model and class 200 using the upper bound model, when performing deterministic bearing capacity assessment.

9.3 Parameter study

As a sensitivity measure the α -vector will be used. The α -vector corresponds to the unit vector for the shortest distance to failure in u -space, and it gives a measure on the relative importance of the stochastic variables. An estimate for the α -vector can be determined by normalizing the realized variables giving failure and putting the normalized mean values into a vector, and then dividing by the magnitude of the vector giving the unit vector. This is illustrated in Figure 9.2. The normalized variable, u , is found from the realized variable x by (9.6),

$$u = \Phi^{-1}(F_X(x)) \quad (9.6)$$

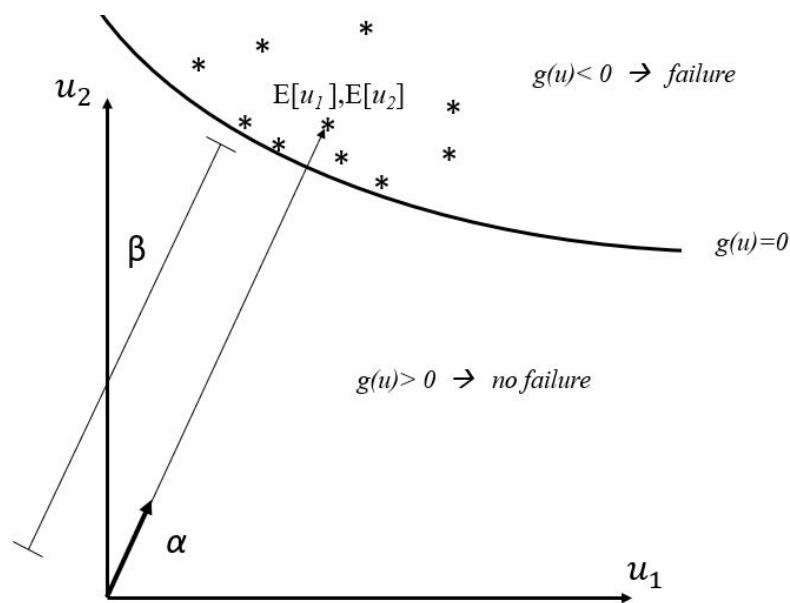


Figure 9.2: Illustration for description of α

For the stochastic variables, the cumulative distribution functions, F_X , are given in Chapter 8. In Chapter 8 probability density graphs are shown for the basic variables with corresponding model uncertainties. These graphs are used to determine $F_X(x)$ in order to create a second α -vector containing an entry for each basic variable with corresponding model uncertainty.

As mentioned earlier 10^8 simulations of (9.2) gave no failures for Østerå Bridge with a class 200 standard vehicle. Therefore instead the α -values are found from (9.3), which includes z . For the 4 stochastic models, α is shown in Figure 9.3 and 9.4. It should be noted that I_G and Δ are included in some of the stochastic models but not all. Figure 9.3 shows the α -values for all stochastic variables individually and Figure 9.4 shows the α -values for the basic variables multiplied by the corresponding model uncertainties. It should also be noted that for stochastic model 1 and 2, only two failures were realized with 10^8 simulations, which means that for these two stochastic models, the estimated α -vector might differ significantly from the actual α -vector.

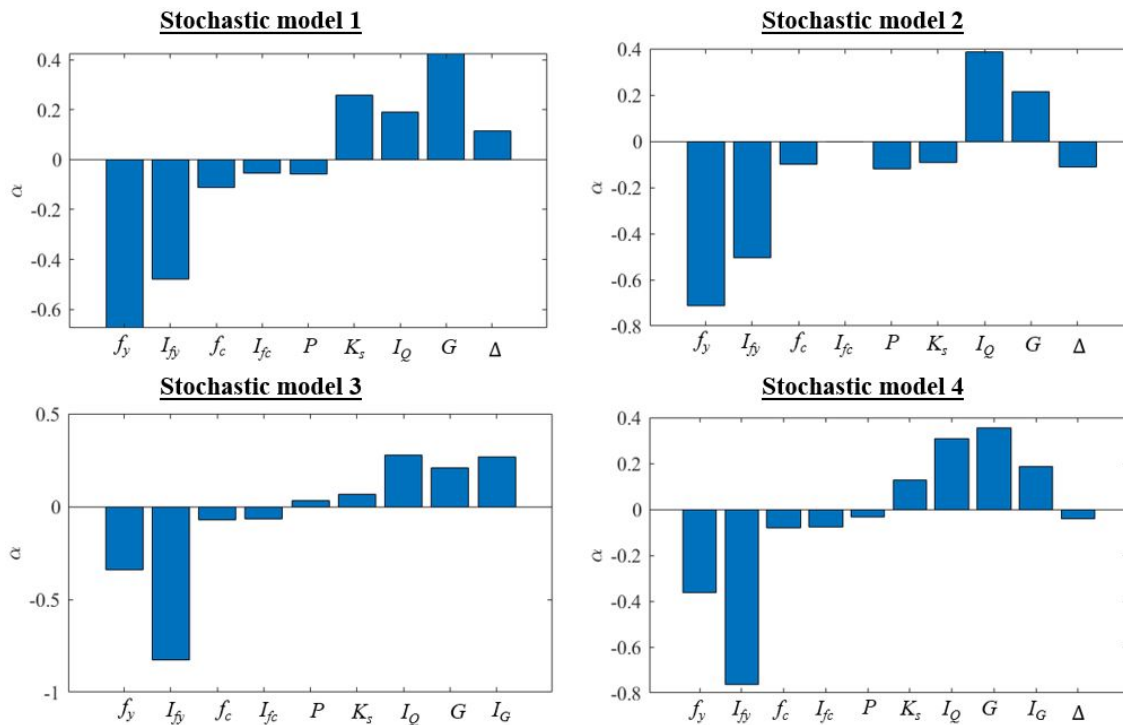


Figure 9.3: α for simulations based on (9.3) with the 4 stochastic models for Østerå Bridge with a class 200 standard vehicle.

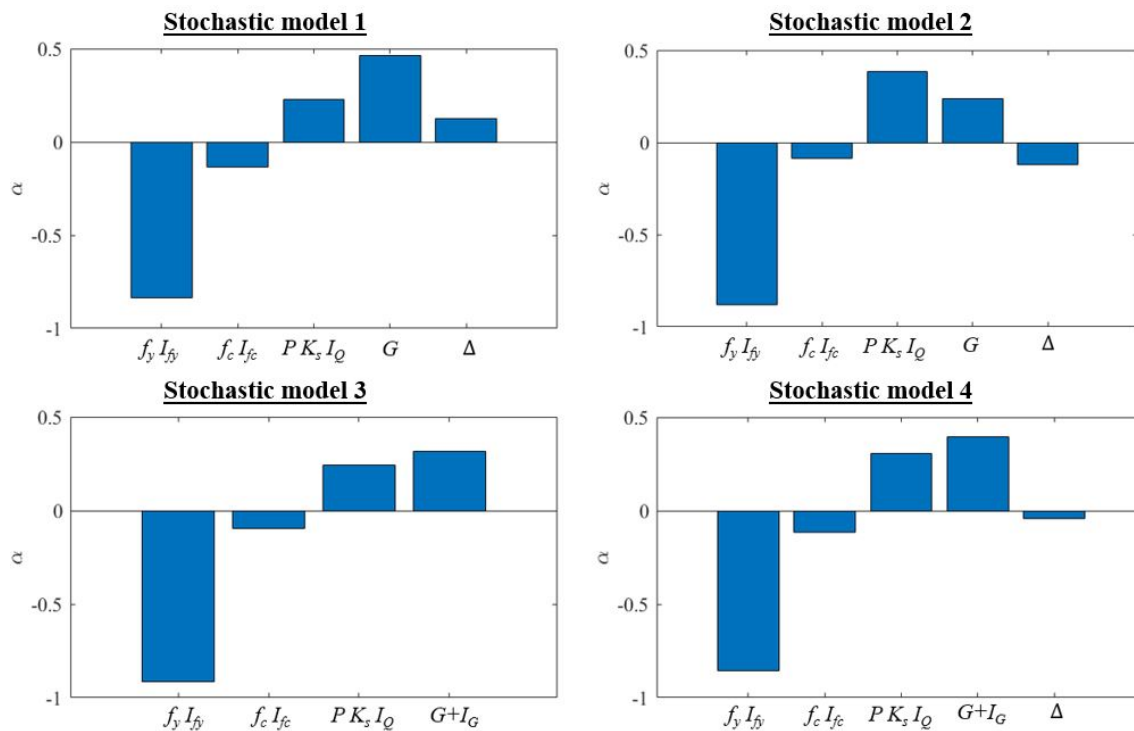


Figure 9.4: α determined based for simulations based on (9.3) with the 4 stochastic models for Østerå Bridge with a class 200 standard vehicle.

It can be seen from Figure 9.3 and 9.4 that for all stochastic models the reinforcement yield stress, f_y , and the respective model uncertainty, I_{f_y} , have high importance. This corresponds to what was deduced from Table 9.1. Furthermore it can be seen that f_y has higher importance than I_{f_y} for model 1 and 2 and vice versa for model 3 and 4. This can be explained by model 1 and 2 having larger COV for f_y and smaller COV for I_{f_y} than model 3 and 4.

Figure 9.3 shows that the dynamic factor, K_s , has little importance in stochastic models 2, 3 and 4. This builds on the statement made earlier in this chapter. However for stochastic model 1 it seems that K_s has higher importance than for the other stochastic models. This however might be due to the low number of realized failures for stochastic model 1 and 2, which increases the uncertainty on the estimated α -vector.

From Figure 9.3 it can be seen that both the concrete strength, f_c , the corresponding model uncertainty, f_c and the annual extreme value vehicle weight, P , have little importance. However the model uncertainty for the traffic load, I_Q , has some importance, which means that $PK_s I_Q$ still has some importance. This can be seen from Figure 9.4

It can be seen from Figure 9.4 that for stochastic model 1, 3 and 4 the permanent load and corresponding model uncertainty, $G + I_G$, has higher importance than the traffic load and corresponding model uncertainty, $PK_s I_Q$. As can be seen from Figure 9.1 the critical failure mechanisms for realized failures are mostly "Partial ellipse". If standard vehicle A is moved closer to the edge, the plastically displaced area of the bridge would probably be reduced, which could result in $PK_s I_Q$ being more important than $G + I_G$.

In Chapter 5 it was hypothesized that the geometry of the bridge and the positioning of standard vehicle A, could have high importance on the reliability of the bridge. This was hypothesized on the basis that the change in C from change in some stochastic variables were higher for some failure mechanisms than others. Since the critical failure mechanism is highly dependent on geometry and traffic load positioning, these parameters might also have influence on the reliability. Therefore as a parameter study, the annual reliability index will be determined for different bridge spans and positions of standard vehicle A in relation to the free edge. Again (9.3) will be used, where z is found from the design equation i.e. z is found from the partial safety factor method. To decrease computation time only stochastic model 1 will be investigated for this. The results are shown in Table 9.3. For illustration of W_Q and L , see Figure 5.5.

Table 9.3: Results for different spans and positions of standard vehicle A on the bridge for stochastic model 1.

W_Q [m]	z	P_f	β	Critical failure mechanism for C_d
L=5m				
0	0.32	$<0.01 \cdot 10^{-6}$	>5.61	Partial ellipse
2.8	0.26	$<0.01 \cdot 10^{-6}$	>5.61	Partial ellipse
8.4	0.25	$<0.01 \cdot 10^{-6}$	>5.61	Full ellipse
14	0.25	$<0.01 \cdot 10^{-6}$	>5.61	Full ellipse
L=9.1m				
0	0.83	$0.01 \cdot 10^{-6}$	5.61	Partial ellipse
2.8	0.74	$0.02 \cdot 10^{-6}$	5.49	Partial ellipse
8.4	0.66	$0.35 \cdot 10^{-6}$	4.96	Partial ellipse
14	0.62	$6.26 \cdot 10^{-6}$	4.37	Full Width
L=13.2m				
0	1.41	$0.11 \cdot 10^{-6}$	5.20	Partial ellipse
2.8	1.33	$2.12 \cdot 10^{-6}$	4.60	Partial ellipse
8.4	1.29	$7.08 \cdot 10^{-6}$	4.37	Full width
14	1.29	$8.91 \cdot 10^{-6}$	4.29	Full width

As it can be seen from Table 9.3, the span of the bridge and the position of the standard vehicle has high importance on the reliability of the bridge, and sufficient reliability is not found for all cases. It can also be seen that when the standard vehicle is moved away from the edge and the failure mechanism before and after are either "Full Ellipse" or "Full Width", z does not change. Otherwise z decreases as the vehicle is moved inward. This is as expected since Figure 5.9 showed that C found for the failure mechanisms "Full Width" and "Full Ellipse" are independent on transverse positioning of the vehicle and that C determined for "Partial Ellipse" increases when the vehicle is moved inward.

Figure 9.5 shows the distribution of C determined for each failure mechanism individually for the cases where the span is $L=9.1$ m but the distance to the edge is changing. In the following a corresponding figure is also shown, but only with the critical failure mechanism.

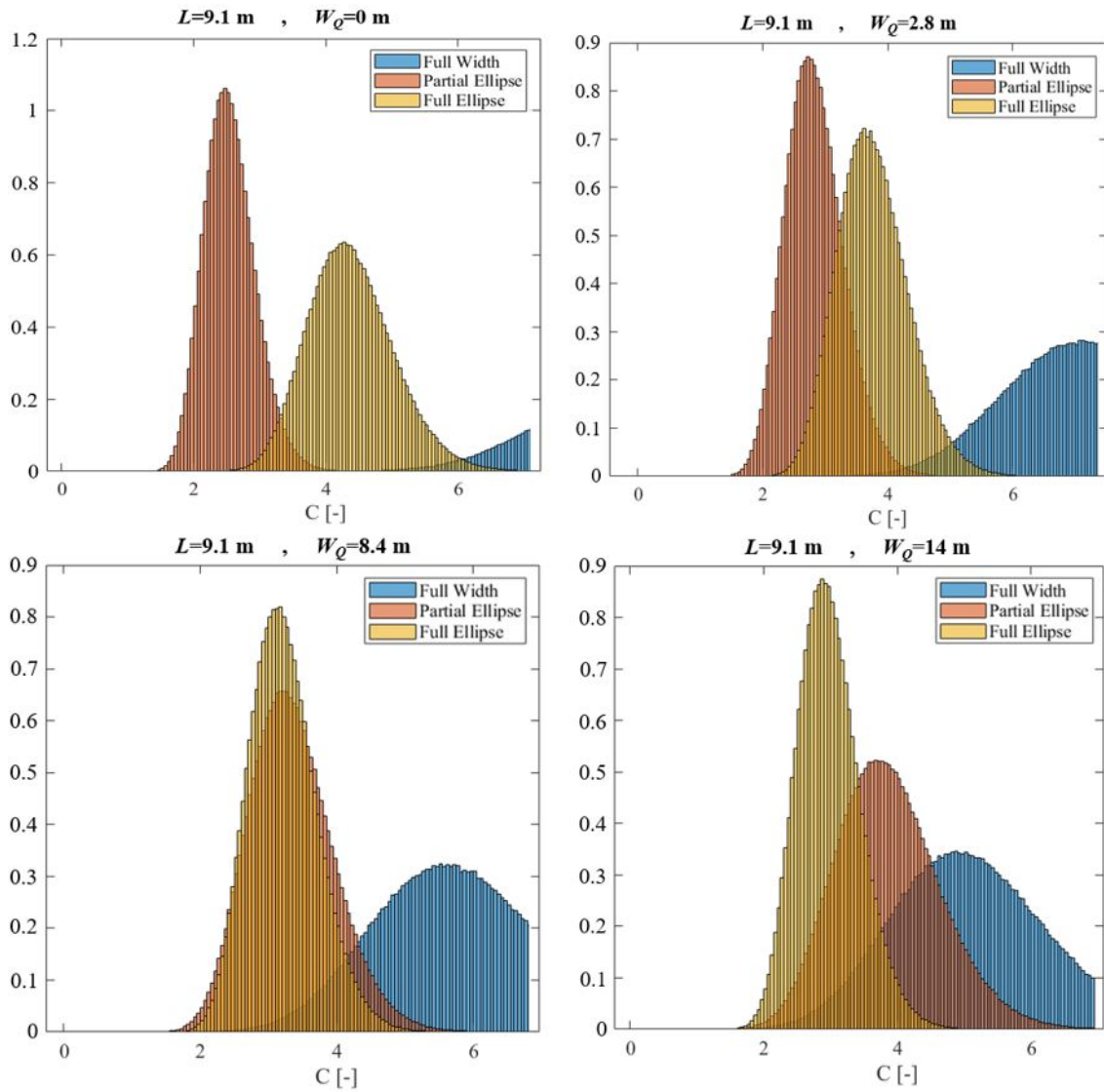


Figure 9.5: Distribution of C determined for each failure mechanism individually for the case where $L=9.1$ m. The histograms are normalized for probability density.

It can be seen from Figure 9.5, that, as expected, C determined for "Full Width" has a larger standard deviation than for the other failure mechanisms. It is also seen that the standard deviation of C determined from "Partial Ellipse" increases as the distance to the edge, W_Q , increases. When W_Q increases the displaced area for "Partial Ellipse" also increases. For "Full Width" the displaced area is the whole slab. This might all suggest that the standard deviation of C increases as a larger part of the total load effect comes from the permanent load. This would also explain, why the annual reliability index determined from the traditional bearing capacity model is larger, since this is calculated as "Full Width" but only for a 3.5 m wide slab.

Figure 9.5 shows that for "Full Ellipse" and "Full width" the mean of C decreases when W_Q increases and that the standard deviation of C increases. These two failure mechanisms should be independent on W_Q , so the change in mean and standard deviation must be due to the decrease in z .

Figure 9.6 shows the distribution of C , and which failure mechanism was critical for the cases where $L=9.1$ m.

Figure 9.6 shows that "Partial ellipse" was critical for all realized failures i.e. $C \leq 1$, when $W_Q = 0$ m, but as W_Q increases more realizations give "Full Width" as the critical failure mechanism. From Table 9.3 it can be seen that more failures are realized when W_Q increases. This is as expected since Figure 9.5 showed that the standard deviation of C determined from "Full Width" was larger than for the other failure mechanisms.

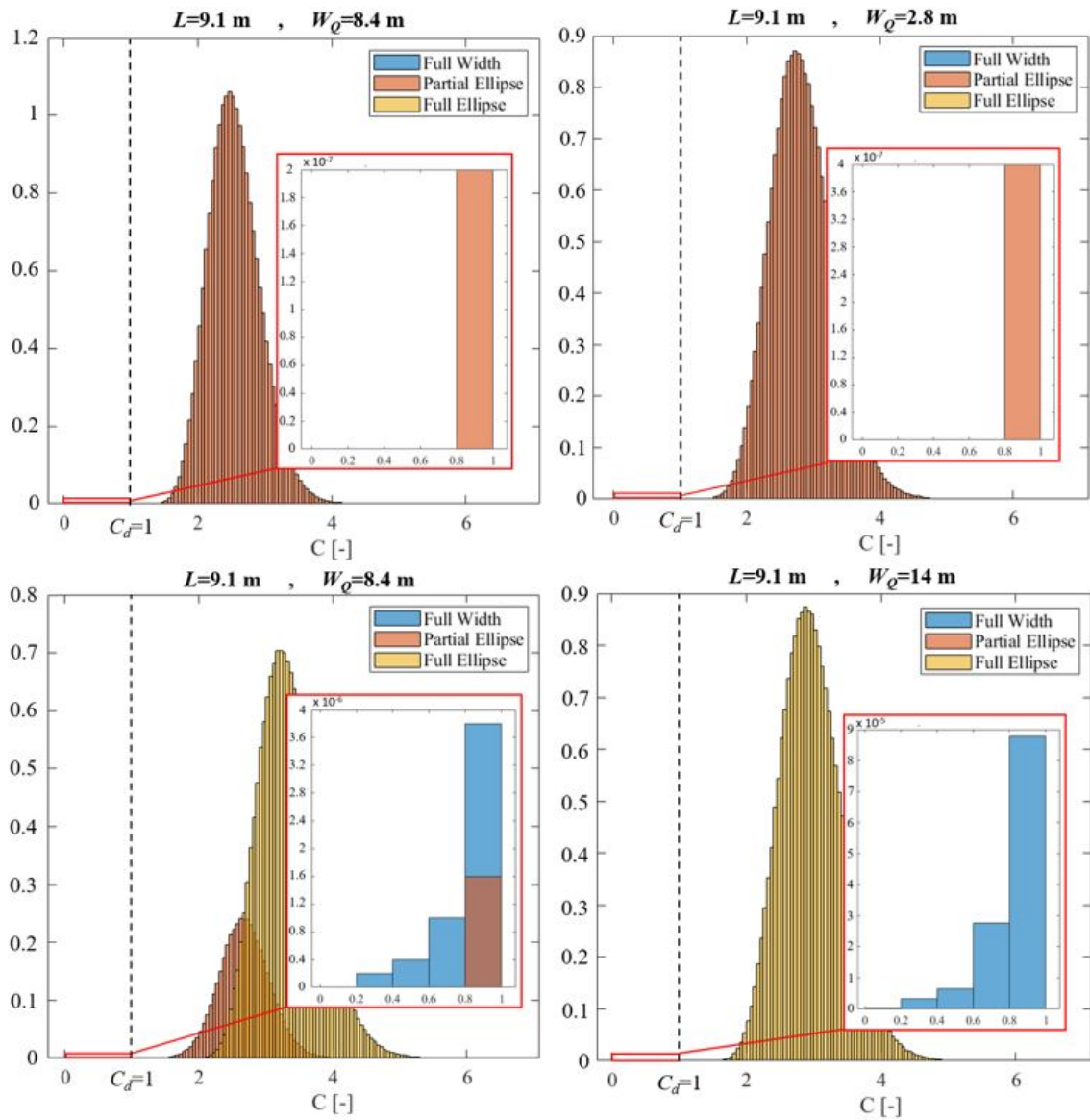


Figure 9.6: Distribution of C , and which failure mechanism was critical for cases where $L=9.1$ m. The histograms are normalized for probability density.

A parameter study is also performed for the span of the bridge, L . Figure 9.7 shows the distribution of C determined for each failure mechanism individually for the cases where the distance to the edge is $W_Q = 2.8$ m but the span is changing.

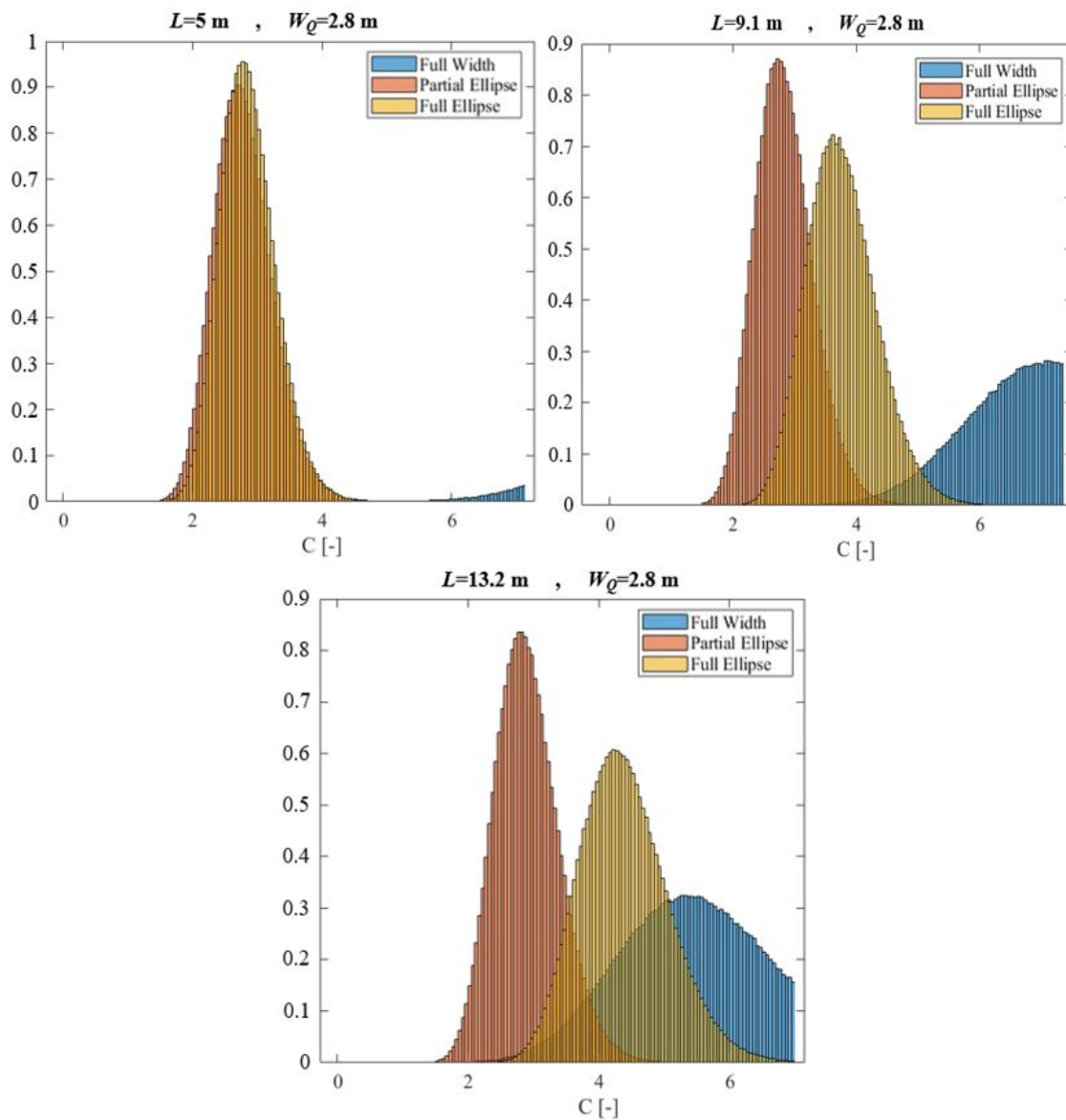


Figure 9.7: Distribution of C determined for each failure mechanism individually for the case where $W_Q = 2.8$ m. The histograms are normalized for probability density.

Figure 9.7 shows that again the failure mechanism giving the highest standard deviation of C is "Full Width", and that the mean of C from "Full Width" decreases with increasing L . It is also seen that the standard deviation of C from "Partial Ellipse" increases slightly with increasing L . These could be the reasons for the reliability index decreasing with increasing L in Table 9.3.

With more time for the project it could be interesting to investigate, if general boundaries for the relevant parameters could be set up, such that the required reliability would always be reached, when using the partial coefficient method with partial coefficients as given in Chapter 2.

10. Proof loading

If the bridge can not be proven for the desired vehicle class through either deterministic or stochastic analysis, it might be proven through proof loading. Furthermore it might be necessary to prove that the classification found from calculation is also applicable in practice, since the upper bound model gives a bearing capacity much higher than what the traditional bearing capacity model gives. However proof loading of the bridge comes with a risk of the bridge failing during the proof loading. When performing the proof load test, devices for measuring strains should be used, so that the proof load test can be stopped before failure happens.

The proof load is the additional load the structure carries during the proof load test besides the permanent load existing before the proof load is applied. Proof loading can be performed by applying dead load to a series of connected hydraulic jacks placed such that the proof loading corresponds to the axle configuration of the standard vehicle for the desired vehicle class. The proof load should be of a magnitude, which, if the bridge survives the proof loading, proves that the annual reliability index of the bridge is larger than or equal to the desired annual reliability index for the given classification. The magnitude of the proof load is found as a factor, η , multiplied to the characteristic extreme value vehicle weight and characteristic dynamic factor, $Q_k K_{s,k}$, such that $\eta Q_k K_{s,k}$ proves the desired annual reliability index. The proof load factor, η , can be found differently based on whether there is prior knowledge on the resistance. In the following sections, η will be determined both for the case with and without knowledge on the resistance.

10.1 Without prior knowledge on resistance

Without prior knowledge on the resistance, the proof load factor will be determined purely from the additional loading. In this case the permanent load is assumed constant, such that the proof load can be determined purely on the basis of the traffic load. However the sensitivity analysis in Chapter 9 showed that the permanent load of the bridge had high importance on the reliability. This means that a small increase in permanent load might mean that the bridge does not reach the desired annual reliability index, when the classification is based on the proof loading factor found without prior knowledge on the resistance

The proof loading factor, η , is determined such that the probability of the traffic load exceeding the proof load, $\eta Q_k K_{s,k}$, is equal to the required annual probability of failure of $P_f = 10^{-6}$. This corresponds to an annual reliability index of $\beta = 4.8$. The annual reliability index with proof loading is determined from the limit state equation (10.1).

$$g = \eta Q_k K_{s,k} - Q K_s I_Q \quad (10.1)$$

Where:

Q	Annual extreme vehicle weight (Characteristic value: 98% quantile).
I_Q	Traffic load model uncertainty
K_s	Dynamic factor
η	Proof loading factor

The annual reliability index and therefore the proof load factor is determined through Monte Carlo simulations. As was described in Chapter 9, 10^8 simulations are performed in order to get sufficient confidence on the estimate.

The proof load factor without knowledge on the resistance is found for vehicle class 50 to 200 for all 4 stochastic models. The results are presented in Table 10.1. As the stochastic variables included in (10.1) have similar distributions in stochastic model 3 and 4, the proof load factor for these models are equal.

Table 10.1: Proof load factor, η , without prior knowledge on the resistance. The values in the parenthesis are the proof loads, $\eta Q_k K_{s,k}$

Standard vehicle class	Stochastic model		
	1	2	3 and 4
50	1.45 (128 ton)	1.27 (112 ton)	1.38 (122 ton)
60	1.42 (143 ton)	1.28 (129 ton)	1.34 (135 ton)
70	1.40 (156 ton)	1.28 (143 ton)	1.32 (147 ton)
80	1.38 (171 ton)	1.28 (159 ton)	1.29 (160 ton)
90	1.36 (190 ton)	1.28 (179 ton)	1.28 (179 ton)
100	1.35 (211 ton)	1.29 (201 ton)	1.26 (197 ton)
125	1.33 (242 ton)	1.29 (235 ton)	1.24 (224 ton)
150	1.32 (283 ton)	1.29 (277 ton)	1.23 (264 ton)
175	1.32 (304 ton)	1.30 (299 ton)	1.23 (283 ton)
200	1.32 (354 ton)	1.30 (348 ton)	1.22 (327 ton)

It can be seen from Table 10.1 that for stochastic model 1, 3 and 4 the proof loading factor decreases with increasing vehicle class. However for stochastic model 2, the proof load factor increases slightly with increasing vehicle weight. The difference might stem from the difference in K_s between the stochastic model 1, 3 and 4, and stochastic model 2. For stochastic model 2 mean and standard deviation of K_s is independent on vehicle weight while the mean and standard deviation of the dynamic factor decreases with increasing vehicle weight for the other models.

For the stochastic variables in (10.1) the only difference between stochastic model 1 and stochastic model 3 and 4 is the distribution type for I_Q . In stochastic model 1 I_Q is Lognormally distributed while I_Q is normally distributed for stochastic model 3 and 4. As can be seen from Table 10.1 the proof load factor is smaller for stochastic model 3 and 4 than for stochastic model 1, which is to be expected.

The method for determination of the proof load factor, which is described in this section, corresponds to the method used in the SBI-guide for assessment of existing structures, [Pedersen, 2015]. This is shown in Appendix D.

If instead the proof load is determined as ηQ_k , the results for η can be seen in Table 10.2.

Table 10.2: Proof loading factor, η , without prior knowledge on the resistance. The values in the parenthesis are the proof loads, ηQ_k

Standard vehicle class	Stochastic model		
	1	2	3 and 4
50	1.78 (128 ton)	1.56 (112 ton)	1.70 (122 ton)
60	1.75 (143 ton)	1.57 (129 ton)	1.65 (135 ton)
70	1.72 (156 ton)	1.57 (143 ton)	1.62 (147 ton)
80	1.70 (171 ton)	1.57 (159 ton)	1.59 (160 ton)
90	1.67 (190 ton)	1.57 (179 ton)	1.57 (179 ton)
100	1.66 (211 ton)	1.58 (201 ton)	1.55 (197 ton)
125	1.64 (242 ton)	1.59 (235 ton)	1.53 (224 ton)
150	1.62 (283 ton)	1.59 (277 ton)	1.51 (264 ton)
175	1.62 (304 ton)	1.60 (299 ton)	1.51 (283 ton)
200	1.62 (354 ton)	1.60 (348 ton)	1.50 (327 ton)

The total weight in Table 10.2 is of course the same as that in Table 10.1, but the proof load factor is just increased proportionally to the characteristic dynamic factor.

10.2 With prior knowledge on the resistance

When there is prior knowledge on the resistance, the proof load factor is conditioned on the assumption on the resistance modelling. The proof load factor is determined such that the probability of the bridge failing during its lifetime given that the bridge survives the proof loading is equal to the required annual probability of failure.

As described in Chapter 9 no failures are realized when performing 10^8 simulations for Østerå Bridge with a class 200 standard vehicle. Therefore the proof load factor can not be determined for Østerå Bridge when only performing 10^8 simulations. A factor, z , will be determined from the design equation. Using this approach η is found as the proof loading factor needed to prove that the result found from deterministic analysis is adequate for up-classification.

A general limit state equation corresponding to failure of the bridge is written as (10.2).

$$g = \min_a \left[\frac{z \sum_{j=1}^{N_y} (m_y(f_y I_{ms}, f_c I_{mc}))_j \theta_j l_j - \int \int_A (I_G + G) \delta(x, y) dx dy}{\sum_{i=1}^{N_F} I_Q K_s P c_{F,i} \delta_i} \right] b \Delta - 1 \quad (10.2)$$

Where:

a	Vector containing different failure mechanisms, as described in Ct 5.
z	Design variable found from design equation
N_y	Number of yield lines
f_y	Yield strength of steel, stochastic
I_{ms}	Model uncertainty on yield strength of steel, stochastic
f_c	Compressive strength of concrete, stochastic
I_{mc}	Model uncertainty on compressive strength of concrete, stochastic
$m_{y,j}$	Yield moment at yield line with index j , stochastic as function of stochastic variables
θ_j	Virtual rotation at yield line with index j
l_j	Length of yield line with index j
A	Deflected area
G	Permanent load, Stochastic
I_G	Model uncertainty of permanent load, stochastic
P	Annual extreme vehicle weight, Stochastic
I_Q	Model uncertainty of traffic load,
K_s	Dynamic factor, stochastic
δ	Virtual deflection
N_F	Number of point loads
$c_{F,i}$	Percentage of extreme value traffic load on i 'th wheel
b	Bias of computation model
Δ	Model uncertainty of computation model, stochastic

The probability of event A given event B can be written as (10.3).

$$P(A|B) = \frac{P(A \cap B)}{P(B)} \quad (10.3)$$

Event A corresponds to failure of the bridge during its lifetime, which from the limit state equation can be determined as (10.4). Event B corresponds to survival of the bridge during the proof loading, which from the limit state equation can be determined as (10.5).

$$A : \quad \min_a \left[\frac{z \sum_{j=1}^{N_y} (m_y(f_y, f_c))_j \theta_j l_j - \int \int_A (I_G + G) \delta(x, y) dx dy}{\sum_{i=1}^{N_F} I_Q K_s P c_{F,i} \delta_i} \right] b \Delta \leq 1 \quad (10.4)$$

$$B : \quad \min_a \left[\frac{z \sum_{j=1}^{N_y} (m_y(f_y, f_c))_j \theta_j l_j - \int \int_A (I_G + G) \delta(x, y) dx dy}{\sum_{i=1}^{N_F} \eta P_k K_{s,k} c_{F,i} \delta_i} \right] b \Delta > 1 \quad (10.5)$$

The design parameter, z , in (10.4) and (10.5) is determined the same way as was described in Chapter 9.

There is a possibility, that the system will fail during the proof loading, which should be taken into concern when choosing to perform a proof loading test or not. The probability of the bridge failing during proof load testing is found by $1-P(B)$.

It is assumed that the knowledge on the resistance is uncertain. This is modelled by modelling the mean and coefficient of variation of both the concrete and reinforcement strengths as stochastic variables in (10.4) and (10.5):

- μ_{f_y} : Lognormal distributed with coefficient of variation, $V_{\mu_{f_y}}$
- μ_{f_c} : Lognormal distributed with coefficient of variation, $V_{\mu_{f_c}}$
- V_{f_y} : Lognormal distributed with coefficient of variation, $V_{V_{f_y}}$
- V_{f_c} : Lognormal distributed with coefficient of variation, $V_{V_{f_c}}$

two levels of uncertainty on the resistance are considered:

- Little uncertainty: $V_{\mu_{f_y}}, V_{\mu_{f_c}} = 0.10$ and $V_{V_{f_y}}, V_{V_{f_c}} = 0.05$
- Large uncertainty: $V_{\mu_{f_y}}, V_{\mu_{f_c}} = 0.20$ and $V_{V_{f_y}}, V_{V_{f_c}} = 0.20$

By acquiring knowledge on the material properties the uncertainty might be reduced. This could for example be done by taking out specimens of the material for testing.

When determining the proof load factor through Monte Carlo simulations, z is determined first. Then 10^8 simulations are performed for (10.4) and (10.5), and then η is found such that the probability $P(A|B)$ is equal to the desired annual probability of failure.

η is found for stochastic model 1, 3 and 4 for a class 200 standard vehicle. It is found using both little and large uncertainty on the resistance. The results for η can be seen from Table 10.3, and the probability of failure during proof loading can be seen from Table 10.4.

Table 10.3: Proof loading factor, η , for class 200 vehicles with prior knowledge on the resistance. The values in parenthesis are values for the proof loads.

Uncertainty on resistance	Stochastic model			
	1	2	3	4
Little	1.12 (300 ton)	1.11 (297 ton)	1.08 (289 ton)	1.06 (284 ton)
Very large	1.19 (319 ton)	1.18 (316 ton)	1.12 (300 ton)	1.11 (300 ton)

Table 10.4: Probability of failure during proof load testing with proof load factors from Table 10.3.

Uncertainty on resistance	Stochastic model			
	1	2	3	4
Little	0.2%	0.2%	0.2%	0.1%
Large	5.1%	4.9%	4.1%	3.5%

Comparing Table 10.1 and 10.3 it can be seen that as expected the proof load factor is smaller when the resistance is taken into account. It can be seen for the case with knowledge on the resistance, that the value of η depends on, which stochastic model is used. This follows what was found for the case without knowledge on the resistance. It can also be seen that the level of uncertainty on the resistance has some importance for the proof load factor. Furthermore by looking at Table 10.4 it can be seen that the level of uncertainty on the resistance also has some importance on the probability of failure during proof load testing. Therefore it might be beneficial to e.g. take out samples of the reinforcement to minimize the level of uncertainty.

For stochastic model 3 and 4, η was the same for the case with no knowledge on the

resistance, since the traffic load model is the same for these two models. However when there is knowledge on the resistance it is seen from Table 10.3 that η is larger for stochastic model 3 than for model 4. Table 9.1 showed that the annual reliability is larger for stochastic model 4 than for model 3, which might explain the difference in η for the two models, when there is knowledge on the resistance.

As mentioned earlier, in this chapter it is investigated how large the proof load factor should be, in order to prove experimentally, that the highest allowable vehicle class found from deterministic analysis gives the required annual reliability. As explained this is done by determining z from the design equation with the desired vehicle class. With more time for the project it would be interesting to determine η and $1-P(B)$ for a case where deterministic analysis could not prove the bearing capacity with the desired vehicle class, but where the desired vehicle class is still to be proven experimentally. This could be done by determining z from the design equation with e.g. a class 175 standard vehicle, and then determining η and $1-P(B)$ with a class 200 standard vehicle. Furthermore the proof load could be investigate for more vehicle classes with more time for the project.

Calculations for the proof load factor are also performed for the traditional bearing capacity model. The results can be seen in Table 10.5 and 10.6.

Table 10.5: Proof loading factor, η , for class 200 vehicles with prior knowledge on the resistance and based on the traditional bearing capacity model. The values in parenthesis are values for the proof loads.

Uncertainty on resistance	Stochastic model			
	1	2	3	4
Little	1.16 (311 ton)	1.15 (308 ton)	1.10 (295 ton)	1.08 (289 ton)
Large	1.21 (324 ton)	1.20 (322 ton)	1.14 (306 ton)	1.13 (306 ton)

Table 10.6: Probability of failure during proof load testing with proof load factors from Table 10.5

Uncertainty on resistance	Stochastic model			
	1	2	3	4
Little	0.6%	0.5%	0.5%	0.2%
Very large	8.3%	7.8%	6.0%	5.3%

Table 10.5 shows that for the traditional bearing capacity model, the proof load factor is generally slightly larger than for the upper bound slab model. As was discussed in Chapter 9, a larger part of the total load effect comes from the traffic load for the traditional model than for the upper bound slab model. Since it is only the traffic load, which changes from event A and B , this might explain the increase of η .

Looking at Table 10.6 it can be seen that the probability of failure during proof loading is larger for the traditional model than for the upper bound model. This could be expected since the proof load is larger, although Chapter 9 showed that the probability of failure during its lifetime was lower for the traditional bearing capacity model.

In Chapter 9 a parameter study was performed to investigate how changes in different parameters affect the annual reliability. Similiarly, this will be done in the following to

investigate the effect on η and $1-P(B)$ of changing different parameters.

10.2.1 Parameter study

For this parameter study, it is investigated how change in the span, L , and distance to the edge, W_Q , affects η and $1-P(B)$. In order to save time, the parameters are only investigated for stochastic model 1 with large uncertainty on the resistance and with a class 200 vehicle. The results can be seen in Table 10.7.

Table 10.7: Results for different spans and positions of standard vehicle A on the bridge for stochastic model 1 with large uncertainty on the resistance. The results are with a class 200 standard vehicle.

W_Q [m]	η	ηQ_k	$1-P(B)$
L=5m			
0	1.18	316 ton	4.4%
2.8	1.17	314 ton	4.6%
14	1.17	314 ton	4.3%
L=9.1m			
0	1.19	319 ton	4.7%
2.8	1.19	319 ton	5.1%
14	1.16	311 ton	5.9%
L=13.2m			
0	1.21	324 ton	5.2%
2.8	1.21	324 ton	5.5%
14	1.18	316 ton	6.0%

Looking at Table 10.7 it seems that as W_Q increases, η decreases. As was discussed in Chapter 9, when W_Q increases a larger part of the total load effect comes from the traffic load. This might explain why η decreases with increasing W_Q , although Table 9.3 showed that the annual reliability was also decreasing with increasing W_Q . Table 10.7 also shows that η increases slightly for increasing L for most cases.

It might be expected that the probability of failure during proof loading, $1-P(B)$, would be largest for the cases with the largest proof load factors in Table 10.7. However this is not the case. If Table 10.7 is instead compared to Table 9.3, it can be seen that as the annual probability of failure increases, the probability of failure during proof load testing also increases.

11. Decision framework for proof loading

Engineering decisions most often rely on the economic aspects of the project. From a socioeconomic viewpoint it might be interesting to investigate the decision on whether to up-classify existing routes, based on the costs and benefits of an up-classification of the existing route. For this project it is however assumed, that the governing bodies already have decided, that an up-classification has to be performed along the route, and that the limiting factor along the route is a bridge, which can not be up-classified based on the traditional bearing capacity model. Furthermore it is assumed, that if bearing capacity assessment using upper bound theory shows, that the bridge can be up-classified, then it should be proven through proof load testing. The decision framework developed in this project is based on bridges, which can be up-classified based on deterministic calculations using the upper bound bearing capacity model. Thereby the probability of failure during proof loading from Chapter 10 can be used for the decision framework. The route can then be up-classified by strengthening the bridge according to traditional bearing capacity models, building a new bridge or up-classifying the bridge based on successful proof load testing. However the proof load testing can also result in failure of the bridge, which means that a new bridge has to be erected. Furthermore the proof load testing can be stopped before the required proof load is reached, which means that the bridge should either be strengthened or a new bridge should be erected. The overall decision tree is illustrated in Figure 11.1.

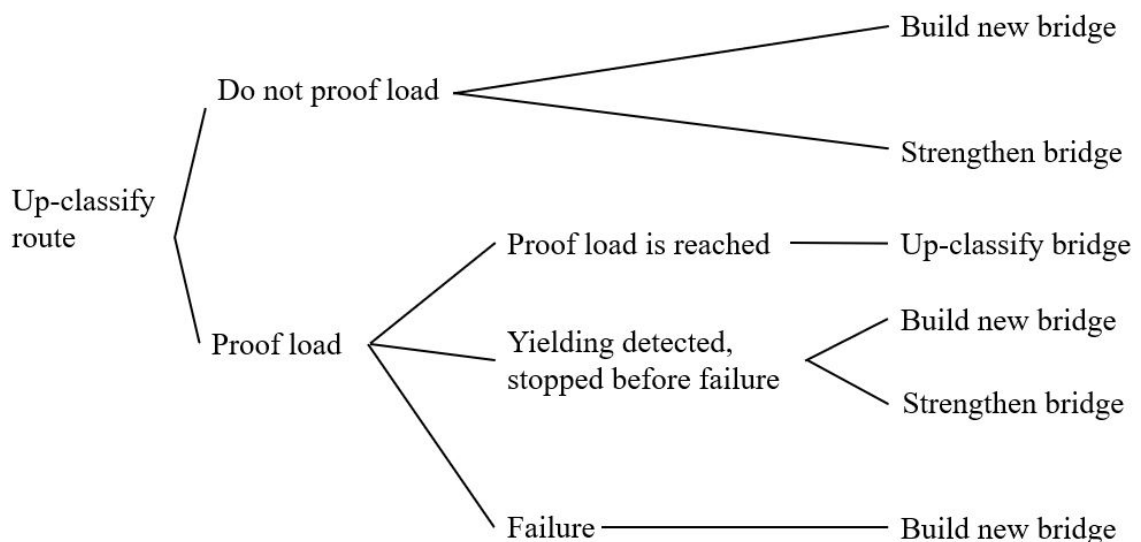


Figure 11.1: Overall decision tree.

Figure 11.1 shows that in some cases there is a choice between strengthening the existing bridge and building a new bridge. In these cases it is assumed that the existing bridge will be strengthened, since this is cheaper. Thereby the decision tree in the figure can be limited to only a decision on whether to proof load test or not. The decision on proof load testing is based on the expected cost of the proof load test, U_1 , and the expected cost of not proof loading, U_0 . To determine these utilities Figure 11.2 is used.

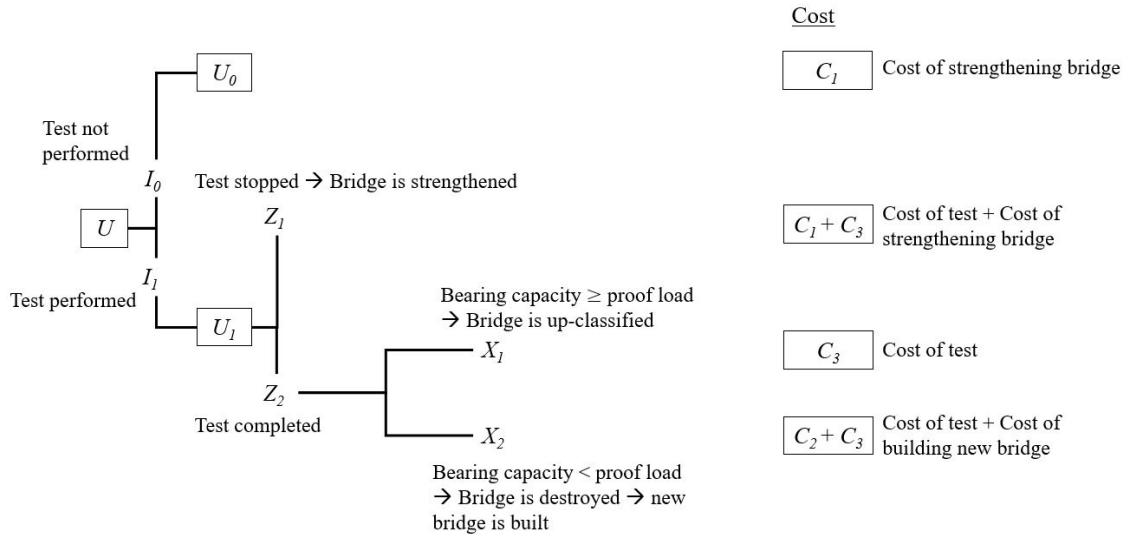


Figure 11.2: Decision tree for decision on proof loading.

The costs and prior probabilities for determining the expected costs are listed in Table 11.1. The expected costs are determined for each of the 4 stochastic models with the different uncertainty levels on the resistance. The probability of failure during proof load testing for these cases can be seen in Table 10.4.

Table 11.1: Proof loading factor, η , for class 200 vehicles with prior knowledge on the resistance. The values in parenthesis are the probability of failure during proof loading.

Parameter		Value
Prob. of bearing capacity \geq proof load	$P(X_1)$	$1 - P(X_2)$
Prob. of bearing capacity $<$ proof load	$P(X_2)$	See Chapter 10
Prob. of stopping the proof load test conditional on bearing capacity \geq proof load	$P(Z_1 X_1)$	0
Prob. of <u>not</u> stopping the proof load test conditional on bearing capacity \geq proof load	$P(Z_2 X_1)$	1
Prob. of stopping the proof load test conditional on bearing capacity $<$ proof load	$P(Z_1 X_2)$	0.99
Prob. of <u>not</u> stopping the proof load test conditional on bearing capacity $<$ proof load	$P(Z_2 X_2)$	0.01
Cost of strengthening existing bridge	C_1	4000 kr/m ²
Cost of building new bridge	C_2	20 000 kr/m ²
Cost of proof load testing	C_3	200 000 kr

As can be seen from Table 11.1 it is assumed that $P(Z_1|X_1)=0$, which means that it is

assumed that the test is only stopped if the bearing capacity is too low to survive the required proof load. This however might be optimistic, and therefore the effect of this on the expected costs will be investigated in a following parameter study. Furthermore it can be seen that the cost of strengthening the bridge or building a new bridge is dependent on the area of the bridge, while cost of the proof load test is a set cost. Therefore this parameter will also be investigated in the parameter study.

The expected cost of not performing the proof load test is just the cost of strengthening the bridge or $U_0 = C_1$. The method for calculating U_1 is shown in Appendix E.

The decision on whether to proof load test or not should of course be taken based on cheapest option. Therefore $U = \min(U_0, U_1)$. Using the probability of failure during proof load testing given in Table 10.4 and the geometry of Østerå Bridge, U_0 and U_1 have been determined, which can be seen in Table 11.2.

Table 11.2: expected cost of not proof load testing, U_0 , and expected cost of proof load testing, U_1 , for different proof load factors and levels of uncertainty found in Table 10.3 and 10.4.

Expected cost	Stochastic model			
	1	2	3	4
Little uncertainty				
U_0	1 205 000 kr	1 205 000 kr	1 205 000 kr	1 205 000 kr
U_1	203 000 kr	203 000 kr	203 000 kr	201 000 kr
Very large uncertainty				
U_0	1 205 000 kr	1 205 000 kr	1 205 000 kr	1 205 000 kr
U_1	264 000 kr	261 000 kr	251 000 kr	244 000 kr

It can be seen from Table 10.4 that for Østerå bridge the expected cost of performing the proof load test is much lower than the expected cost of not performing the proof load test. This is true for all stochastic models and levels of uncertainty. Of course U_0 does not change, as this is independent on the probability of failure during proof load. However as both the probability of failure during proof load testing and the costs given in Table 11.1 are dependent on the geometry of the bridge, investigations for the area are made in the parameter study.

As U_1 is much lower than U_0 for all cases in Table 11.2 it might also be interesting to investigate how the expected costs would be affected if the proof load test was performed for vehicle classes larger than what could be proven for by the partial safety factor method. However for this the corresponding proof load factor and $P(X_2)$ would have to be determined in order to determine U_1 , which is time demanding. With more time for the project, this could have been investigated. This was also discussed for further work in Chapter 10. Instead in the following parameter study, it will just be investigated how changes in $P(X_2)$ will affect the expected costs.

11.1 Parameter study

As mentioned earlier, in this parameter study the effect on the expected costs from changing the area, $P(X_2)$ and $P(Z_2|X_1)$ will be investigated. The results for this can be seen in Figure 11.3 for stochastic model 1 with large uncertainty on the resistance and the geometry of Østerå Bridge.

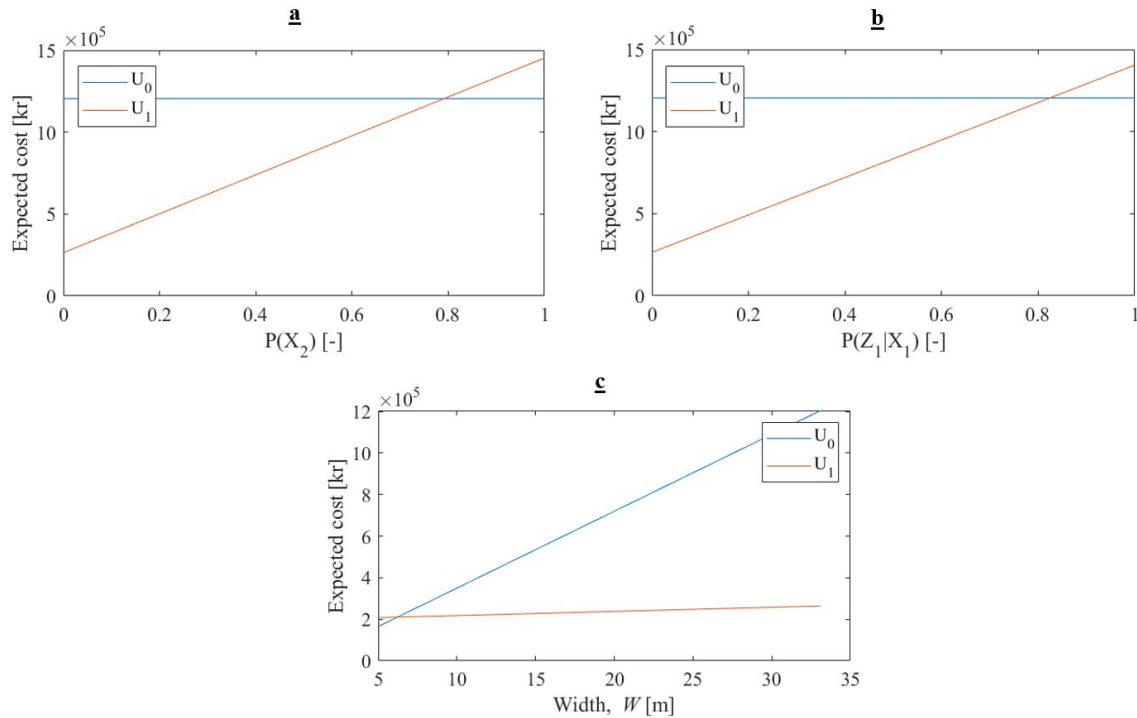


Figure 11.3: Effect on expected costs of change in different parameters.

Figure 11.3a shows that $P(X_2)$, which is the probability that the bearing capacity is smaller than the required proof load, can be almost 0.8 before U_1 becomes larger than U_0 . This might suggest that there could be something to be gained if instead the proof load test was performed for vehicle classes larger than what could be proven for by the partial safety factor method.

From Figure 11.3b it can be seen that $P(Z_1|X_1)$, which is the probability of the proof load being stopped conditional on the bearing capacity being larger than the proof load, is around 0.8 before U_1 becomes larger than U_0 . This could suggest that although $P(Z_1|X_1) = 0$ might be optimistic, with the costs and the other probabilities in Table 11.1, this parameter does not have much importance for the decision on proof load testing.

As was mentioned earlier in this chapter, the area of the bridge might be important for the decision on proof load testing, since some of the costs in Table 11.1 are dependent on the area. In Figure 11.3c the width of the bridge and thereby the area is reduced. As can be seen from the figure, the width can be reduced from 33.1 m to almost 5 m before U_1 becomes larger than U_0 .

12. Conclusion

The purpose of this report was to investigate how plastic upper bound theory could be used for up-classification of short span bridges. This was investigated for both deterministic, reliability-based and experimental bearing capacity assessment. A bridge, which in this report is designated Østerå bridge, was used as a base case for the calculations, and parameter studies were performed in relevant chapters.

From the load models of the existing norms, it was found that the traffic load of a given vehicle class, was to be applied as a concentrated point load for each wheel of the standard vehicle. The whole weight of the vehicle should be distributed onto the wheels, with a set percentage for each wheel. From plastic upper bound theory a method for determining the bearing capacity based on this traffic load was developed. It was found, that through upper bound plasticity theory, the bearing capacity could be determined as a factor, C , which is the ratio between the applied traffic load, and the traffic load leading to failure. In the parameter study it was found that three of the considered failure mechanisms could each be critical depending on parameters, such as width of the bridge or reinforcement yield stress. What was found to be interesting from the parameter study, was that changes in the loads and strength parameters affected C differently depending on the failure mechanism. This meant, that since strengths and loads were stochastic variables in the reliability-based bearing capacity assessment, that the mean and standard deviation of C would differ depending on the critical failure mechanism.

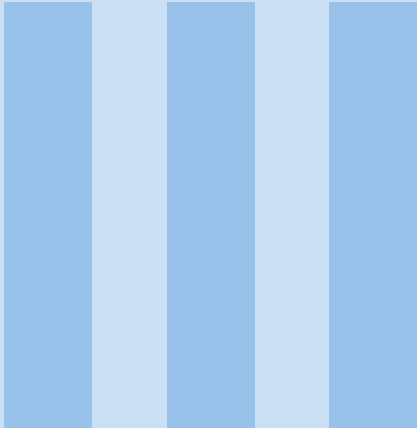
For Østerå Bridge bearing capacity assessment was performed with the partial safety factor method for both the developed upper bound model and for a more traditional model. Calculations using the traditional model showed that Østerå bridge could be classified for class 100 vehicles, which is also what the bridge is classified for at the time of this report. On the other hand calculations using the developed upper bound model showed that the bridge could be classified for class 200 vehicles, which are the heaviest vehicles investigated for in this report, and moreover that $C = 2.8$ using a class 100 vehicle.

The required annual probability of global failure for existing bridges is $P_f = 10^{-6}$. The reliability method used for the reliability-based bearing capacity assessment was Monte-Carlo simulations with 10^8 simulations. For Østerå bridge none of the 10^8 gave failure when using a class 200 vehicle, which meant that the bridge could also be classified for class 200 vehicle on the basis of reliability-based assessment. The reliability-based method was compared to the partial safety factor method for Østerå Bridge using 4 different stochastic models, and it was found for 3 of the stochastic models, that the reliability-based method could potentially give higher classification than the partial safety factor method. However it was hypothesized from the parameter study, that this was highly dependent on how much of the total load effect was from the traffic load and the permanent load, respectively.

For experimental bearing capacity assessment a proof load factor, which is needed for classification based on proof load tests, was determined taking into account knowledge on the resistance. This was again based on the upper bound model and Monte Carlo simulations. It was determined as a factor multiplied to the characteristic traffic load, giving the required proof load, such that if the bridge survived the proof load, the required annual reliability would be proven. The proof load was found as the proof load needed to prove that the reliability of the bridge with the desired vehicle class was sufficient if the partial safety factor method showed that the bridge could be classified for the desired vehicle class. With this it was found that the required proof load factor was lower, when taking into account knowledge on the resistance. The probability of failure during the proof load was also determined, and this was used to investigate the decision on proof loading. It was found that the expected cost of proof loading was much lower than the expected cost of not proof loading, if partial safety factor method showed that the bridge could be classified for the desired vehicle class. Further work could be done, where the decision on proof loading could be investigated if analytic methods could not prove the bridge for the desired vehicle class.

Bibliography

- Andersen, 2017.** Ulrik Andersen. *Vejbroer kan bære meget mere, end man troede*. Ingeniøren, 2017.
- DS/EN-1990, 2007.** DS/EN-1990. *Eurocode 0 - Basis of structural design*, 2007.
- DS/EN 1991-2 DK NA:2017, 2017.** DS/EN 1991-2 DK NA:2017. *National Anneks til Eurocode 1: Last på bærende konstruktioner - Del 2: Trafiklast på broer*, 2017.
- Google, 2020.** Google. *Google Earth*, 2020.
- Jensen, 2012.** Bjarne Chr. Jensen. *Betonkonstruktioner efter DS/EN 1992-1-1*. ISBN: 978-87-571-2766-9. Nyt Teknisk Forlag, 2012.
- Jensen and Bonnerup, 2014.** Bjarne Chr. Jensen and Bent Bonnerup. *Plasticitetsteori, 2. udgave*. ISBN: 978-87-571-2807-9. Nyt Teknisk Forlag, 2014.
- Optum, 2020.** Optum. *Optum MP*, 2020.
- Pedersen, 2015.** Erik Steen Pedersen. *SBI-ansøgning 251, Vurdering af eksisterende konstruktioners bæreevne*. ISBN: 978-87-563-1660-6. Statens byggeforskningsinstitut, 2015.
- Sørensen, 2016.** Professor John Dalsgaard Sørensen. *Undersøgelser vedr. partialkoefficienter og dynamiske forstærkningsfaktorer for særtransporter*, 2016.
- Sørensen, 2009.** Professor John Dalsgaard Sørensen. *Baggrundsundersøgelser ifm. udarbejdelse af brospecifikke Nationale Annekser til Eurocodes EN1990 og EN1991*, 2009.
- Vejdirektoratet, 2004.** Vejdirektoratet. *Reliability-based classification of the load carrying capacity of existing bridges*. ISBN: 87-7923-774-6, report 291. Road Directorate, 2004.
- Vejdirektoratet, 2017.** Vejdirektoratet. *Vejledning til belastnings- og beregningsgrundlag for broer*. <http://vejregler.lovportaler.dk/showdoc.aspx?t=%2fV1%2fNavigation%2fTillidsmandssystemer%2fVejregler%2fAnlaegsplanlaegning%2fBygvaerker%2fBelastninger%2f&docId=vd20170137-full>, 2017.



Appendix

- A** Axle configuration for standard vehicles 77
- B** Bearing capacity calculation example 79
- C** Cases for determination of model uncertainty 83
- D** Proof load factor for existing structures 87
- E** Calculation of expected cost 89

A. Axle configuration for standard vehicles

Klasse	Akselkonfiguration Akseltryk i tons og akselafstande i m	Sporvidde m
10		2,6
20		2,6
30		2,6
40		2,6
50		2,6
60		2,6
70		2,6
80		2,6
90		2,6
100		2,6
125		2,8
150		2,8
175		2,8
200		2,8

Figure A.1: Axle configuration for standard vehicles. [Vejdirektoratet, 2004]

B. Bearing capacity calculation example

In this chapter the bearing capacity will be calculated for a specific failure mechanism. The specific failure mechanism is "PartialBox" with dimensions and loading as shown in Figure B.1. The slab is additionally loaded by a uniformly distributed load, G_k .

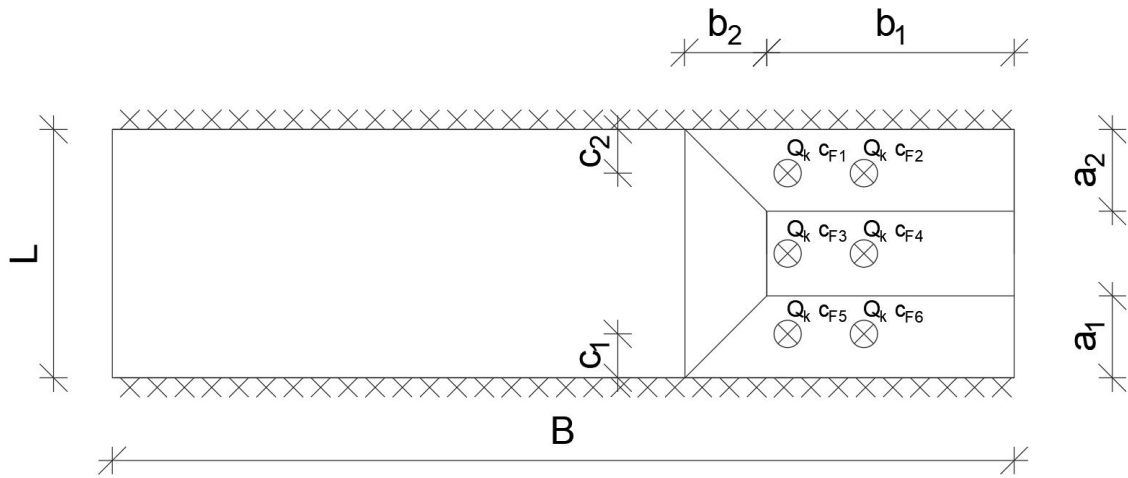


Figure B.1: Example of yield lines with loading for the failure mechanism, "PartialBox"

As shown in the main report the bearing capacity, C , is generally calculated by the expression:

$$C = \frac{\sum_{j=1}^{N_y} m_{yk,j} \theta_j l_j - \int \int_A G_k \delta(x,y) dx dy}{\sum_{i=1}^{N_F} Q_k c_{F,i} \delta_i}$$

$$C = \left[\frac{\sum_{j=1}^{N_y} (m_{yk}(f_{yk}, f_{ck}))_j l_j \theta_j - \int \int_A G_k \delta(x,y) dx dy}{\sum_{i=1}^{N_F} Q_k c_{F,i} \delta_i} \right] \quad (B.1)$$

In the following is shown how each part of this equation, is expanded into corresponding expressions for the specific case. For the parts corresponding to the outer work and thereby the loads, Figure B.2 is used. The four displaced areas are assigned roman numerals in order to easier show the relation between the figure and the expressions.

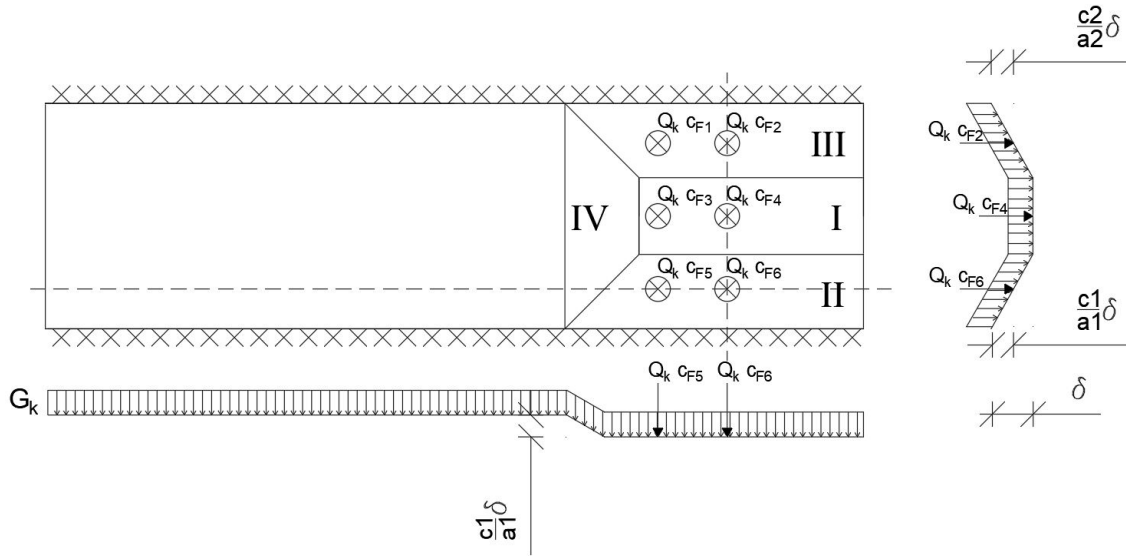


Figure B.2: Figure for determination of the outer work.

The maximum virtual displacement of the failure mechanism is equal to a virtual displacement, δ , which corresponds to the displacement of area I, as can be seen from Figure B.2. The displacement at any other point is determined from this as each of the displaced areas are assumed to be rigid bodies. The outer work performed by the concentrated loads can then be expressed as:

$$\sum_{i=1}^{N_F} Q_k c_{F,i} \delta_i = Q_k c_{F1} \frac{c_2}{a_2} \delta + Q_k c_{F2} \frac{c_2}{a_2} \delta + Q_k c_{F3} \delta + Q_k c_{F4} \delta + Q_k c_{F5} \frac{c_1}{a_1} \delta + Q_k c_{F6} \frac{c_1}{a_1} \delta$$

The outer work performed by the uniformly distributed load, G_k , can be expressed as:

$$\begin{aligned} \int \int_A G_k \delta(x,y) dx dy &= \underbrace{G_k b_1 (L - a_1 - a_2)}_I \delta + \underbrace{G_k \left(a_1 b_1 \frac{\delta}{2} + \frac{a_1 b_2}{2} \frac{\delta}{3} \right)}_{II} \\ &+ \underbrace{G_k \left(a_2 b_1 \frac{\delta}{2} + \frac{a_2 b_2}{2} \frac{\delta}{3} \right)}_{III} \\ &+ \underbrace{G_k \left((L - a_1 - a_2) b_2 \frac{\delta}{2} + \frac{a_1 b_2}{2} \frac{\delta}{3} + \frac{a_2 b_2}{2} \frac{\delta}{3} \right)}_{IV} \end{aligned}$$

For determination of the inner work Figure B.3 is used. The reinforcement is assumed as both an upper and lower grid with reinforcement lying in transverse and longitudinal directions. Therefore the determination of the inner work is based on the yield moments arising from the four yield moments shown in the figure. Each yield moment is assigned a name with the index after yk corresponding to the direction of the reinforcement (t for transverse and l for longitudinal).

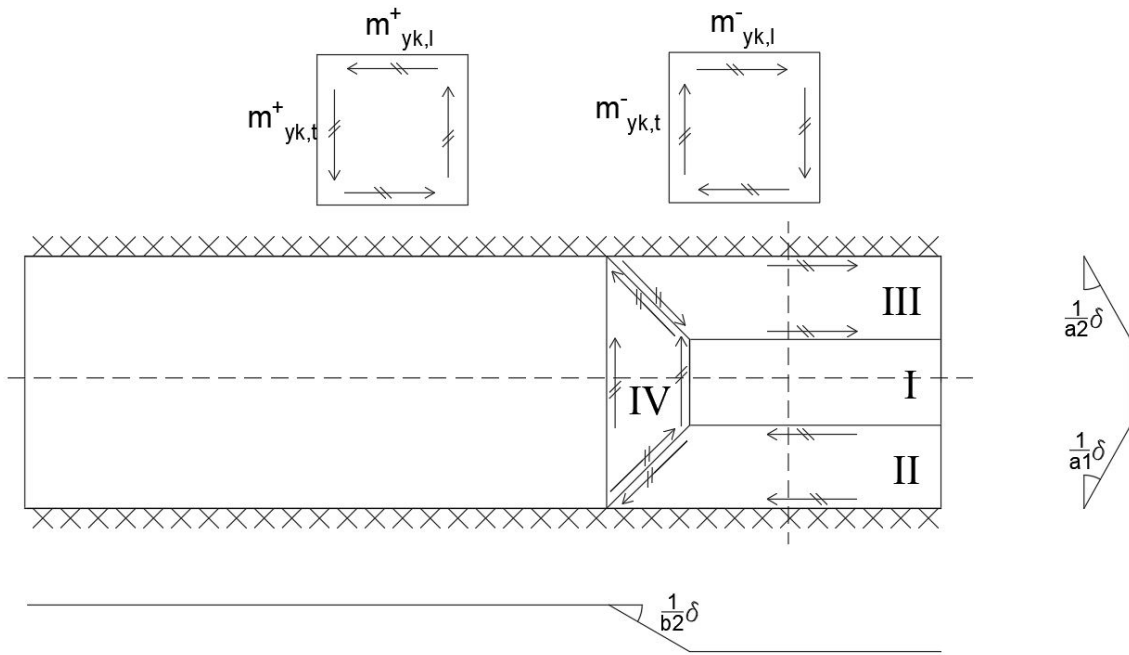


Figure B.3: Figure for determination of the inner work.

The inner work is expressed by:

$$\sum_{j=1}^{N_y} m_{yk,j} l_j \theta_j = \underbrace{(m_{yk,l}^+ + m_{yk,l}^-)}_{\text{II}} (b_1 + b_2) \frac{1}{a_1} \delta + \underbrace{(m_{yk,l}^+ + m_{yk,l}^-)}_{\text{III}} (b_1 + b_2) \frac{1}{a_2} \delta + \underbrace{(m_{yk,t}^+ + m_{yk,t}^-)}_{\text{IV}} L \frac{1}{b_2} \delta$$

In some cases the axis of rotation doesn't run along the transverse or longitudinal direction, as illustrated in Figure B.4. In such a case as the one illustrated the inner work is calculated by:

$$\sum_{j=1}^{N_y} m_{yk,j} l_j \theta_j = \left(\sqrt{(m_{yk,l}^+ \cos v)^2 + (m_{yk,t}^+ \sin v)^2} + \sqrt{(m_{yk,l}^- \cos v)^2 + (m_{yk,t}^- \sin v)^2} \right) a \frac{1}{b} \delta \quad (\text{B.2})$$

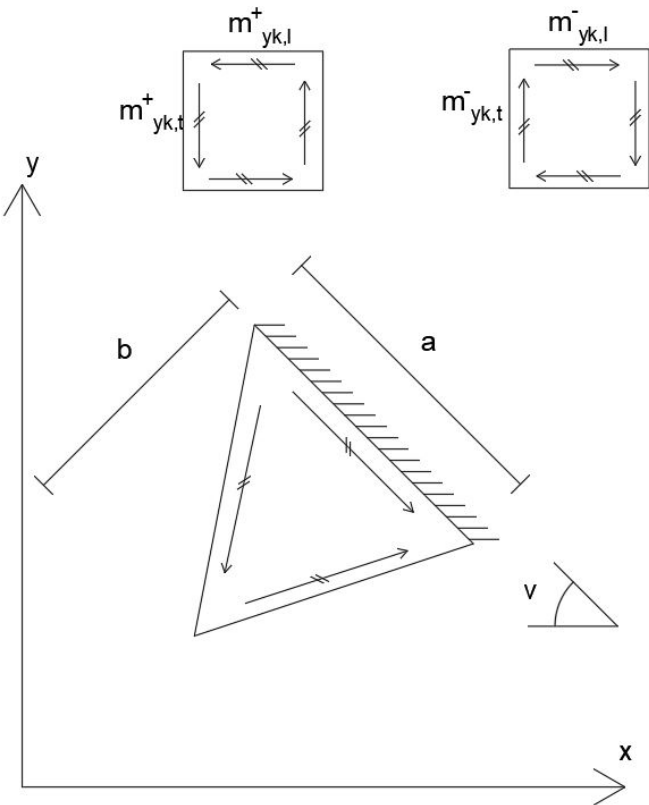


Figure B.4: Figure for determination of the inner work.

C. Cases for determination of model uncertainty

L=9.1 m						
Test no.	d [m]	B [m]	Dead load [kPa]	Yield stress [MPa]	C _t [-]	C _e [-]
1	6	33.1	35.6	623	7.28	6.75
2	6	33.1	39.1	623	7.07	6.63
3	6	33.1	35.6	573	6.50	6.11
4	6	33.1	39.1	573	6.26	5.99
5	6	33.1	35.6	523	5.70	5.47
6	6	33.1	39.1	523	5.46	5.30
7	6	14.5	35.6	623	7.28	6.75
8	6	14.5	39.1	623	7.07	6.63
9	6	14.5	35.6	573	6.50	6.11
10	6	14.5	39.1	573	6.23	5.99
11	6	14.5	35.6	523	5.67	5.47
12	6	14.5	39.1	523	5.33	5.30
13	7	33.1	35.6	623	7.28	6.75
14	7	33.1	39.1	623	7.15	6.63
15	7	33.1	35.6	573	6.57	6.11
16	7	33.1	39.1	573	6.43	5.99
17	7	33.1	35.6	523	5.85	5.47
18	7	33.1	39.1	523	5.72	5.30
19	4.5	12	35.6	623	6.20	6.19
20	4.5	12	39.1	623	5.91	5.90
21	4.5	12	35.6	573	5.44	5.44
22	4.5	12	39.1	573	5.16	5.14
23	4.5	12	35.6	523	4.69	4.68
24	4.5	12	39.1	523	4.41	4.40
25	5.5	14	35.6	623	7.04	6.81
26	5.5	14	39.1	623	6.82	6.63
27	5.5	14	35.6	573	6.27	6.05
28	5.5	14	39.1	573	6.02	5.82
29	5.5	14	35.6	523	5.47	5.30
30	5.5	14	39.1	523	5.14	5.06
31	12	33.1	35.6	345	3.34	3.14
32	12	33.1	39.1	345	3.19	3.00
33	12	33.1	35.6	295	2.63	2.47
34	12	33.1	39.1	295	2.39	2.33
35	12	33.1	35.6	245	1.62	1.51
36	12	33.1	39.1	245	0.91	0.90

L=12 m						
Test no.	d [m]	B [m]	Dead load [kPa]	Yield stress [MPa]	C _t [-]	C _e [-]
37	12	33.1	35.6	623	4.63	4.25
38	12	33.1	39.1	623	4.45	4.07
39	12	33.1	35.6	573	4.10	3.78
40	12	33.1	39.1	573	3.76	3.61
41	12	33.1	35.6	523	3.42	3.26
42	12	33.1	39.1	523	3.01	2.85
43	4.5	19	35.6	623	3.38	3.20
44	4.5	19	39.1	623	3.16	2.97
45	4.5	19	35.6	573	2.92	2.73
46	4.5	19	39.1	573	2.61	2.56
47	4.5	19	35.6	523	2.37	2.33
48	4.5	19	39.1	523	1.92	1.91
49	4.5	17	35.6	623	3.36	3.20
50	4.5	17	39.1	623	2.95	2.94
51	4.5	17	35.6	573	2.74	2.73
52	4.5	17	39.1	573	2.33	2.33
53	4.5	17	35.6	523	2.12	2.12
54	4.5	17	39.1	523	1.73	1.72

D. Proof load factor for existing structures

In the SBI-guide 251, [Pedersen, 2015], proof load factors are given for existing structures with 1 variable load, where there is no knowledge on the resistance. The procedure for how these proof load factors are determined corresponds to the procedure described in Chapter 10. In this chapter, the procedure used for [Pedersen, 2015] will be shown.

The proof load is determined such that the probability, that the additional action on the structure is larger than or equal to the proof load, is equal to the desired probability of failure. By additional action is meant the load, not including the permanent load from before the proof loading test, which will be applied to the structure. The proof load factor, η , is determined as a factor multiplied to the characteristic additional load, S_k , giving the proof load ηS_k . The characteristic additional load is the permanent load added to the structure after the proof load test, G , and the variable load, Q applied to the structure. S_k is given by (D.1).

$$S_k = (1 - \alpha) G_k + \alpha Q_k \quad (\text{D.1})$$

α is included in (D.1) to determine a proof load factor dependent on the percentage of the additional load coming from the variable load. The limit state equation for determination of η is given by (D.2).

$$g = S_k \eta - ((1 - \alpha) G + \alpha Q) \quad (\text{D.2})$$

The distribution parameters for G and Q can be seen from Table D.1.

Table D.1: Distribution parameters for G and Q .

Parameter		Distribution type	COV	Characteristic, fractile
Permanent load	G	Normal	0.1	50 %
Variable load	Q	Gumbel	0.4	98 % (2.04 μ_Q)

A Gumbel distribution is given by (D.3), where parameters a and b are determined from (D.4) and (D.5).

$$F_X(x) = \exp(-\exp(-a(x - b))) \quad (\text{D.3})$$

$$a = \frac{\pi}{V\sqrt{6}} \quad (\text{D.4})$$

$$b = \mu - \frac{0.5772}{a} \quad (\text{D.5})$$

In determination of η , the variable load and the permanent load are normalized with respect to the characteristic values. This means that G_k and Q_k are set to 1. To determine η , 10^9 simulations are performed for G and Q . For the permanent load, $\mu_G = G_k = 1$. For simulations of Q , the mean is set to $\mu_Q = Q_k/2.04 = 1/2.04 = 0.49$. η is determined for different α -values, such that the probability of failure for (D.2) is equal to the desired probability of failure. The results are listed in Table D.2.

Table D.2: Values for the proof load factor, η .

α	$\beta=3.2$	$\beta=3.8$	$\beta=4.3$	$\beta=4.7$	$\beta=5.2$
0	1.52	1.85	2.19	2.48	2.87
25	1.39	1.65	1.89	2.11	2.40
50	1.28	1.45	1.61	1.75	1.95
60	1.24	1.38	1.51	1.62	1.78
65	1.22	1.34	1.46	1.56	1.69
70	1.20	1.31	1.41	1.50	1.61
75	1.20	1.29	1.37	1.44	1.54
80	1.20	1.27	1.34	1.40	1.48
85	1.21	1.28	1.33	1.37	1.43
90	1.24	1.30	1.34	1.38	1.43
95	1.28	1.34	1.38	1.42	1.47
100	1.32	1.38	1.43	1.47	1.52

The values in Table D.2 are exactly the same as the values given for the proof load factor in [Pedersen, 2015].

E. Calculation of expected cost

The expected cost of proof load testing, U_1 , can be determined from Figure E.1.

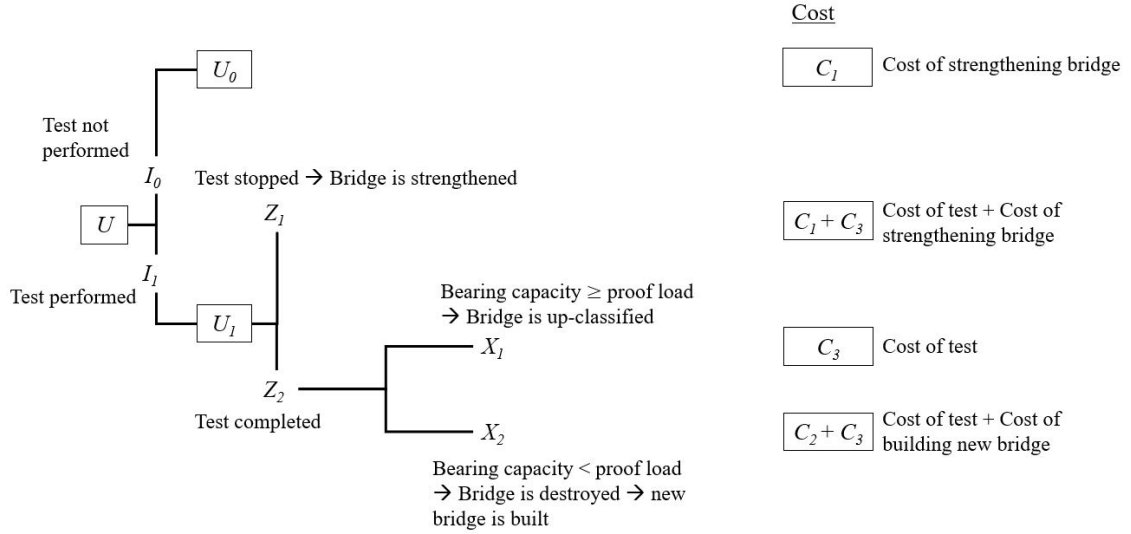


Figure E.1: Decision tree for decision on proof loading.

U_1 is determined from (E.1).

$$U_1 = P(Z_1) (C_1 + C_3) + P(X_1|Z_2)P(Z_2) C_3 + P(X_2|Z_2) P(Z_2) (C_2 + C_3) \quad (E.1)$$

The probabilities $P(X_1|Z_2)$ and $P(X_2|Z_2)$ can be determined by (E.2) and (E.3).

$$P(X_1|Z_2) = \frac{P(Z_2|X_1)P(X_1)}{P(Z_2|X_1)P(X_1) + P(Z_2|X_2)P(X_2)} \quad (E.2)$$

$$P(X_2|Z_2) = \frac{P(Z_2|X_2)P(X_2)}{P(Z_2|X_1)P(X_1) + P(Z_2|X_2)P(X_2)} \quad (E.3)$$

The probabilities $P(Z_1)$ and $P(Z_2)$ is determined from (E.4)

$$P(Z_i) = P(Z_i|X_1)P(X_1) + P(Z_i|X_2)P(X_2) \quad (E.4)$$

